View metadata, citation and similar papers at core.ac.uk

brought to you by CORE

provided by NASA Technical Reports Server

The University of Alabama in Huntsville

Annual Report for Grant NAG8-834
Due Date: June 24, 1992

"Theoretical and Experimental Studies Relevant to Interpretation of Auroral Emissions"

Submitted to

George C. Marshall Space Flight Center
Space Science Laboratory
National Aeronautics and Space Administration
Marshall Space Flight Center, AL 35812

by

Charles E. Keffer
Principal Investigator
The University of Alabama in Huntsville
Physics Department
Huntsville, AL 35899

(NASA-CR-190521) THEORETICAL AND EXPERIMENTAL STUDIES RELEVANT TO INTERPRETATION OF AURORAL EMISSIONS Annual Report (Alabama Univ.) 66 p

N92-28911

Unclas
G3/46 0108048

Table of Contents

1. **Introduction** 1

2. **Space Vehicle Environment Study** 1
   - 2.1 **Radiation Testing** 2
   - 2.2 **Thermal Testing** 5
   - 2.3 **Flight Filter Measurements** 6
   - 2.4 **UVI Calibration** 7

3. **Auroral Modeling** 7
   - 3.1 **Integration of Models** 7
   - 3.2 **Auroral Model Updates** 8
   - 3.3 **High Latitude Extensions** 10
   - 3.4 **Conductivity Calculations** 10
   - 3.5 **UVI Workshops** 12

4. **References** 13

5. **Appendix A - Radiation Test Results** 14

6. **Appendix B - Semiannual Status Report** 59

Theoretical and Experimental Studies Relevant to Interpretation of Auroral Emissions

1. Introduction

In recent years, there has been an increasing awareness of the fragile balance required to maintain the Earth's environment in a healthy condition. The Earth's upper atmosphere and its interaction with the solar environment is recognized as playing a crucial role in maintaining this balance. Despite a rapidly increasing data base of knowledge on the Earth's atmosphere much remains to be learned. Optical emissions from upper atmospheric constituents represent a fundamental tool for understanding both the composition and the physical processes which contribute to the ability of the atmosphere to sustain a high quality of life on the Earth. Space-based observation platforms are frequently able to make measurements of upper atmospheric emissions which are either impossible to make from the ground or superior to their ground-based counterparts. Specifically, auroral imaging from a space-based platform makes it possible to determine the total auroral energy influx and the characteristic energy of the incident auroral particles. In addition, it is possible, through modeling, to map and relate these parameters from the thermosphere/ionosphere to the various regions of the Earth's magnetosphere.

This report summarizes the results obtained in the second year of a three year collaborative effort with MSFC. A succession of experimental studies has been completed to determine the effects of the natural and induced space vehicle environment on the measurement of auroral images from spaced-based platforms. In addition, a global model which incorporates both auroral and dayglow emission sources is being developed to allow interpretation of measured auroral emissions. A description of the work completed on these two tasks follows.

2. Space Vehicle Environment Study

In this second year of effort the experimental portion of this study has begun to concentrate on the effect of the natural and induced space environment for the Ultraviolet Imager (UVI). The UVI is a part of the International Solar Terrestrial Physics (ISTP) mission to study the Earth's magnetosphere. The UVI will be on a polar orbiting satellite which will be exposed to the high radiation environment of space during its three year nominal mission lifetime. In addition, the thermal environment of space is critical to the UVI since it is passively cooled by radiative heat transfer from a thermal radiator on the instrument to the 3 °K thermal background of space. Laboratory tests have been conducted to determine the performance of the UVI in its anticipated radiation and thermal environments. Measurements of reflectance and transmittance have also been completed on all of the UVI flight filters and work is in progress on calibration of the complete instrument.

2.1 Radiation Testing

A set of all-dielectric multilayer interference reflection and transmission filters are being designed and fabricated for the optical system of the Ultraviolet Imager (UVI). The UVI filters will be exposed to the severe radiation environment of space during the nominal three year mission lifetime of the Global Geospace Science Polar spacecraft. The anticipated radiation dose for the UVI filters is < 250 krads. Previous laboratory studies of high-energy radiation damage to optical materials for ultraviolet wavelengths have been limited primarily to transmittance measurements of uncoated substrates.[1-6] It is unknown, therefore, to what extent, if any, the radiation environment to which the UVI will be exposed may damage the filters in flight. We have consequently performed a series of tests to simulate the anticipated radiation dose and to measure its impact on the UVI filters.

We have selected 14 single layer thin films, 4 uncoated substrates, 2 multilayer transmission filters, and 2 multilayer reflection filters for radiation testing. Seven of the single layer thin films, 2 of the uncoated substrates, and all of the multilayer filters were exposed to 250 krads of radiation from a ^{60}Co gamma radiation source at Goddard Space Flight Center. The remaining 9 samples were not exposed to the ^{60}Co source and served as controls. Table 1 contains a matrix of the 22 samples used with the substrate and thin film type shown together with the UVI filter to which it is similar. The radiation and control samples are also identified in Table 1. The complete set of samples is analogous to the substrates, thin films, and filters which make up the UVI optical system.

A series of reflectance and transmittance measurements has been performed on the 22 samples shown in Table 1. The preradiation measurements were performed in a hydrocarbon-free cryopumped vacuum chamber at a pressure below 10^{-5} Torr. A deuterium lamp with a MgF_2 window together with a 0.2-m vacuum monochromator provided 1 nm FWHM spectral resolution over the 120 nm to 180 nm wavelength range. Folding and collimating optics and a 6 mm diameter aperture limited the light incident on the eight position filter wheel holding the 12.5 mm diameter substrates to an area approximately 1/4th the area of the thin film. A photomultiplier tube with a MgF_2 window and a semi-transparent Cs-I photocathode served as the detector for all measurements. The postradiation measurements were accomplished in another hydrocarbon-free cryopumped vacuum chamber also at a pressure below 10^{-5} Torr. A similar deuterium lamp, 0.2-m vacuum monochromator, and aperture were used for the postradiation measurements. However, the second chamber did not have any folding and collimating optics. The same Cs-I photomultiplier tube and eight position filter wheel was used for both the pre- and postradiation measurements. Reflectance measurements were performed at a 45° angle of incidence while transmittance was measured at normal incidence. Figures 1 and 2 illustrate the optical configurations for the two vacuum chambers employed.

For the reflection measurements, two identical scans from 1200 Å to 1800 Å were performed on each substrate prior to their radiation exposure. Filter RF135L/GII was measured as a control on every reflection measurement to check the reliability and reproducibility of the data from scan to scan. The RF135L/GII control insured that no systematic errors were

Sample	Substrate	Coating	Radiation/ Control	UVI Filter
Al_2O_3 1/2	Fused Silica	Al_2O_3	Radiation	TSOLAR
Al_2O_3 2/2	Fused Silica	Al_2O_3	Control	none
BaF_2 1/2	MgF_2	BaF_2	Radiation	T1304,T1356,TLBHS
BaF_2 2/2	MgF_2	BaF_2	Control	none
CaF_2 1/2	MgF_2	CaF_2	Radiation	none
CaF_2 2/2	MgF_2	CaF_2	Control	none
F14-A	MgF_2	BaF_2,MgF_2	Radiation	none
Fused Silica uncoated 1/2	Fused Silica	none	Radiation	TLBHL,TSOLAR
Fused Silica uncoated 2/2	Fused Silica	none	Control	none
HfO_2 1/2	MgF_2	HfO_2	Radiation	none
HfO_2 2/2	MgF_2	HfO_2	Control	none
LaF_3 1/2	MgF_2	LaF_3	Radiation	R1304,R1356,RLBHS, RLBHL,T1304,T1356, TLBHS
LaF_3 2/2	MgF_2	LaF_3	Control	none
MF45-C	MgF_2	BaF_2,MgF_2	Radiation	none
MgF_2 1/2	MgF_2	MgF_2	Radiation	all
MgF_2 2/2	MgF_2	MgF_2	Control	none
MgF_2 uncoated 1/2	MgF_2	none	Radiation	none
MgF_2 uncoated 2/2	MgF_2	none	Control	none
RF135L/B	Fused Silica	LaF_3/MgF_2	Radiation	none
RF135L/D	Fused Silica	LaF_3/MgF_2	Radiation	none
SiO_2 1/2	MgF_2	SiO_2	Radiation	TLBHL
SiO_2 2/2	MgF_2	SiO_2	Control	none

Table 1. Summary of coatings and measurements.

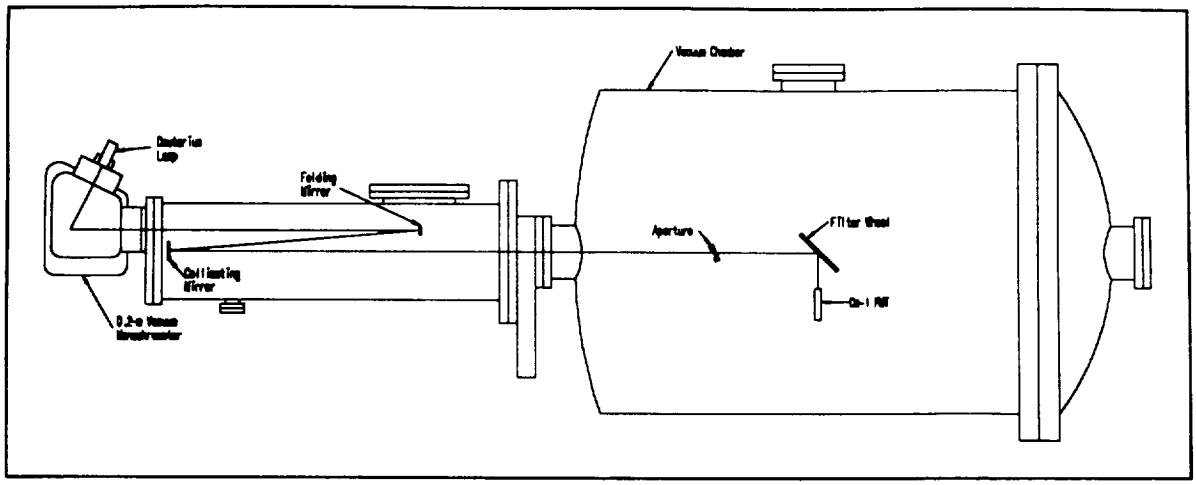

Figure 1. Optical configuration for preradiation measurements.

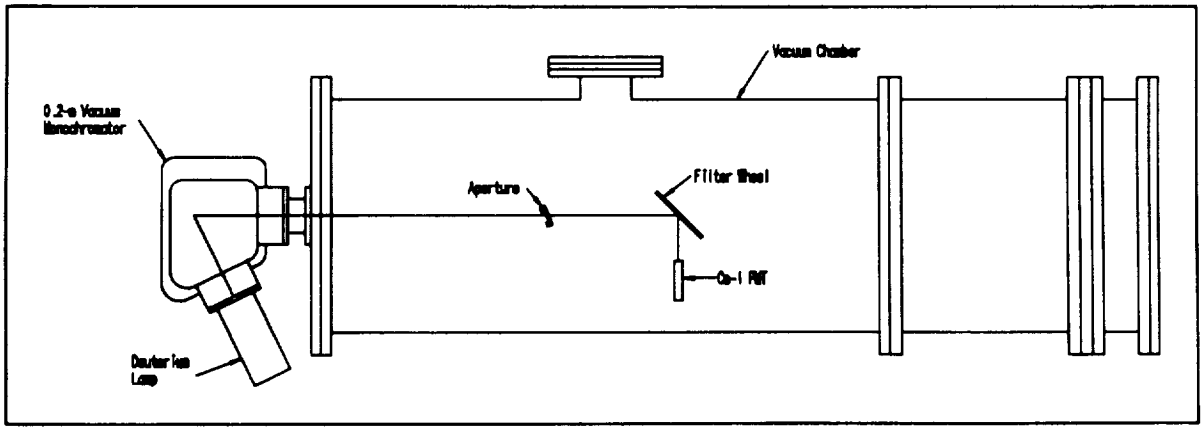

Figure 2. Optical configuration for postradiation measurements.

introduced when the vacuum chamber was vented and a new set of substrates was installed. Two identical scans from 1200 Å to 1800 Å were also performed on each substrate during the transmission measurements. Filter MgF_2 17 was measured on every transmission measurement as a check on the scan to scan reliability and reproducibility. The RF135L/GII and MgF_2 17 filters also provided traceability between the two vacuum chambers used in the pre- and postradiation measurements.

The complete radiation test results are contained in Appendix A - Radiation Test Results. Included are 44 figures showing pre- and postradiation reflectance and transmittance measurements for each of the 22 samples. Each figure shows two measurements before and two measurements after radiation exposure with the data and standard deviation plotted. Also shown are the difference, defined as preradiation minus postradiation, and the ratio, defined as postradiation divided by preradiation.

Repeated measurements of the RF135L/GII and MgF_2 17 filters have led to an estimated run to run uncertainty (2σ) of approximately ± 3%. Of the 44 figures in the Appendix, only 5 show differences which are clearly outside this range of uncertainty. These are CaF_2 2/2 (T), F14A (T), MF45-C (T), MgF_2 uncoated 1/2 (T), and MgF_2 uncoated 2/2 (T). CaF_2 2/2 and MgF_2 2/2 were not irradiated and so could not have experienced any radiation induced damage. The difference in their pre- and postradiation measurements is most likely due to the poorer signal-to-noise ratio of the preradiation measurements. The two filters, F14A and MF45-C, could have experienced some loss in transmission due to their radiation exposure. However, the fact that the ratio of the pre- and postradiation measurements is nearly constant with wavelength indicates that a measurement error may have occurred since radiation damage would likely cause distinct absorption bands to develop[1]. The MgF_2 uncoated sample has a pre- and postradiation measurement difference which is slightly outside the measurement uncertainty, but since the postradiation transmittance is larger than the preradiation transmittance, radiation exposure is an unlikely cause.

In summary, it appears that none of the samples tested have experienced any major radiation induced changes in reflectance or transmittance. Since the UVI filters are made exclusively from materials which we have tested, it is anticipated that they will suffer less than approximately 5% loss in reflectance or transmittance during their nominal 3 year mission lifetime.

2.2 Thermal Testing

Radiative coupling between the UVI and the 3 °K thermal background of space is designed to meet the critical cooling requirements for the instrument. These include a CCD detector temperature below - 55 °C for noise reduction, an optical bench temperature near room temperature to prevent misalignments caused by thermal expansion or contraction, and heat removal from "hot" electronic parts to prevent failures.

The crucial nature of these requirements mandates thorough testing of the full instrument. A vacuum chamber setup was designed and fabricated for this purpose. The UVI was mounted on a baseplate which was temperature controlled over the range of - 20 °C to 30 °C using a recirculating ethanol/water mixture. A second cold plate was mounted approximately 2" above the radiator of the UVI. This cold plate was painted black to increase its emissivity and cooled to approximately 77 °K using flowing liquid nitrogen. Several thermistors and thermocouples monitored the temperature at strategic locations.

A preliminary thermal test was completed in November and December, 1991 using the UVI Engineering Model. Only the Camera portion of the Imager was included in the test since an Electronic Stack was not available at the time. The critical issues were addressed through a sequence of tests with the major results summarized as follows. With the UVI turned on and the cooling systems operational, the hottest electronic parts in the detector remained below 30 °C indicating that they were adequately cooled. Measurements of the optical bench showed that it was difficult to maintain its temperature at or above 22 °C with the available heater power. The CCD cooling was found to be less efficient than desired with its temperature being approximately 5 °C warmer than anticipated. With the Imager in its survival mode, the detector electronics maintained a satisfactory temperature of - 15 °C.

Results of the preliminary thermal test were presented and discussed at the Ultraviolet Imager Thermal Design Review on December 19, 1991. The underlying conclusion of the Review was that differences between the Engineering Model and the Flight Model should be sufficient to correct the problems encountered. A follow-up test using the Flight Model will be necessary to confirm this conclusion. Also, a heater will be placed in front of the instrument to simulate the effect of the sun on the baffle since this was not included in the preliminary test.

The required follow-up thermal test is in progress as of the date of this report.

2.3 Flight Filter Measurements

The UVI is designed to measure atomic oxygen auroral emissions at 1304 Å and 1356 Å, N_2 Lyman-Birge-Hopfield (LBH) auroral emissions from 1400 Å to 1600 Å and from 1600 Å to 1800 Å, and the solar spectrum from 1800 Å to 2100 Å. High sensitivity at the selected wavelength coupled with a high rejection ratio for other wavelengths is required. This optical selectivity is accomplished using the combined throughput of three reflection filters and one transmission filter for each wavelength of interest.

The success of the UVI optical system depends on the correct design and performance of these filters. Accordingly, measurements have been completed of the reflectance or transmittance of all of the flight filters. The measurements were completed in the same manner as the radiation test measurements and using a setup similar to that illustrated in Figure 2. The R130-1-1 reflection filter (1304 Å) measurement shown in Figure 3 is typical of the results obtained.

As of the date of this report, measurements have been completed on 35 of the 40 flight filters and spares verifying their correct design and performance.

2.4 UVI Calibration

The calibration of the UVI is essential to its successful usage in making quantitatively accurate measurements of auroral emissions. A calibration procedure has been written detailing the required measurements. These include the measurement of absolute sensitivity, flat field response, wavelength dependence, angular dependence and temperature dependence. Experimental setups have been designed and fabricated for each of the required calibration tests. Preparations are in progress for completion of these tests.

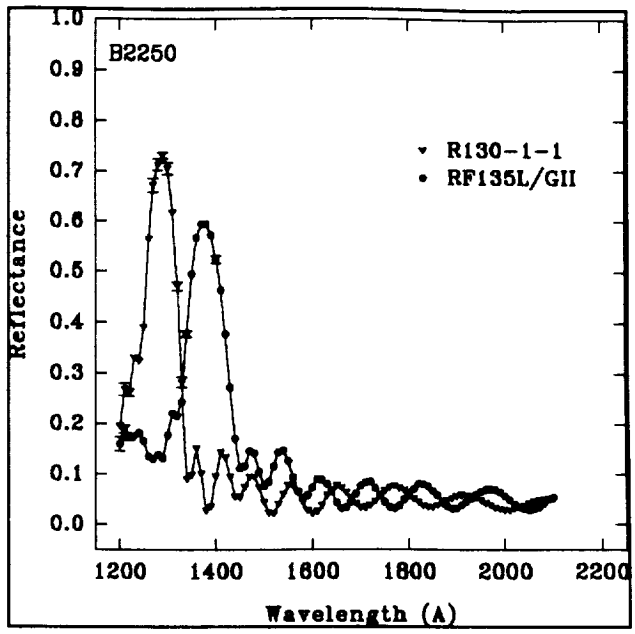

Figure 3. R130-1-1 flight filter reflectance measurement.

3. Auroral Modeling

The principal modeling goals for the past year were to continue the integration of the Field Line Interhemispheric Plasma (FLIP) and auroral codes, to extend the use of the FLIP model into the high latitude auroral regions, to develop an ionospheric conductivity algorithm, and to convene the second UVI workshop for discussion of analysis of auroral images. As detailed below, we have successfully achieved each of these goals.

3.1 Integration of Models

The integration of our two-stream auroral code with the global FLIP model is central to the modeling aspect of this program. The auroral electron code accurately models energy degradation of an incident electron flux and resultant auroral emissions. It has no knowledge, however, of the chemistry and dynamics of the global ionosphere-thermosphere. The FLIP model, on the other hand, is an excellent representation of these processes but does not include the auroral processes. A combination of the two models will allow simultaneous modeling of auroral emissions superimposed on underlying airglow. With the recent implementation of new versions of both models, this goal is complete.

The updated FLIP model now accepts auroral production data from the auroral model as standard input data. Since the two codes exchange information through ASCII intermediate files, it is now possible to run different segments of the combined code on different platforms. For example, we now use the power of the MSFC CRAY computer for the compute-intensive

sections of the FLIP code while using the more rapid turn-around of a VAX system for the smaller auroral sections. The overall result is a more efficient modeling system.

The combined codes are currently used to compare the intensity of modeled FUV auroral emissions with that of anticipated dayglow emissions as they would be seen from space. Previously, FUV auroral images have been presented for large solar zenith angles, with little work being done for images seen against a full midday airglow background. This is largely because previous FUV filter technology was such that adequate blocking of scattered visible sunlight could not be achieved. The next generation of FUV imagers, however, will incorporate ultraviolet filters both sufficiently narrow to allow separation of the FUV features of interest and with adequate blocking throughout the visible and near infrared to prevent out-of-band contamination. Accordingly, we are presently modeling FUV auroral emissions against a superimposed dayglow as a function of both solar zenith angle (SZA) and incident energy flux.

3.2 Auroral Model Updates

In addition to the combination of the auroral and FLIP models we have modified the auroral code to include an important additional source of auroral 1356 Å emission. Most models, including our previous codes, have only considered a single source of O(^{5}S) 1356 Å emission, namely electron impact excitation of O. There is, however, an additional potential source of 1356 Å emission, the dissociative excitation of molecular oxygen by electron impact. Dissociative excitation of O_2 by electrons is a significant source of OI 7774 Å emission for hard auroral spectra.[7] We can reasonably assume that the same mechanism may also be important in the production of auroral 1356 Å emission. Dissociative excitation cross sections for 1356 Å have been reported[8] but these have not generally been included in auroral codes. Our studies, however, indicate this is a significant source of auroral 1356 Å emission and should be included in any representation of the auroral processes.

In Figure 4 we show the excitation cross sections for 1356 Å production by electron impact on atomic and molecular oxygen. The crosses are the cross sections for excitation of atomic oxygen used in our model. The solid circles give the cross sections reported by Wells et al.[8] and the solid curves are the parameterizations to these values used in our models. (Only the parameterization above the peak energy is shown for the e+O process.) The peak value of the Wells et al.[8] cross section is virtually the same, to within reported error limits, as the peak value we are using for the e+O cross section. Furthermore, the e+O_2 cross section is quite broad. Both these facts imply that we can expect a significant increase in 1356 Å emission from dissociative excitation by auroral electrons. Note that dissociative excitation will be significant only for auroral electrons. Photoelectrons are typically produced with energies below that of the peak e+O_2 cross section. Thus the production of 1356 Å dayglow by photoelectron dissociative excitation of O_2 is small.

In Figure 5 we show modeled auroral 1356 Å integrated column brightnesses with and without the addition of the dissociative excitation source from O_2. With the e+O 1356 Å source alone, only auroral electrons whose energies have degraded to below about 40 eV can

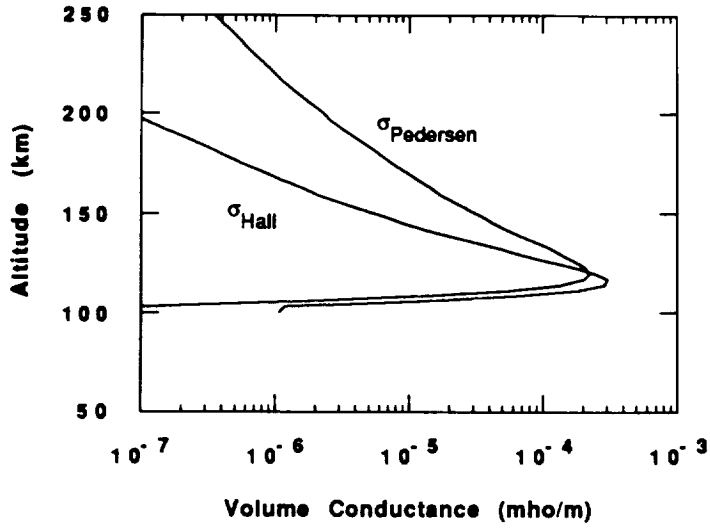

Figure 6

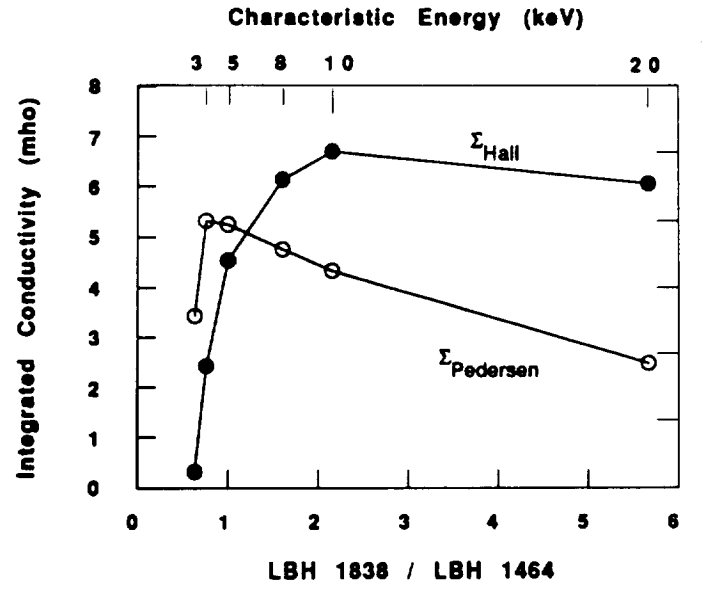

Figure 7

significantly contribute to 1356 Å production. With the addition of the $e+O_2$ source, auroral electrons produce 1356 Å emission throughout the energy cascade process. The result is a significant increase in the 1356 Å column intensity with the additional excitation source. This difference is about a factor of 2 at 10 keV.

3.3 High Latitude Extensions

The FLIP model is a closed field line model and assumes, incorrectly, that the field lines remain closed throughout the polar regions. Attempts to model these regions with closed field lines lead to infinitely large field lines and attendant computational difficulties. We had previously thought the FLIP model would have to be modified to include open field lines. Our work under this grant has shown, however, that a good model of the airglow can be obtained by turning off the field-line diffusive solutions in the FLIP code. This has the advantage of using the existing code with minimal modification.

In addition to being able to run at polar latitudes, the FLIP model must also be modified to take account of several high latitude mechanisms. One of the more significant mechanisms is the drift of ionospheric plasma due to local electric fields. Plasma convection throughout the polar region can significantly alter the plasma densities relative to a static model which has the feet of the flux tubes anchored to the Earth's surface. Plasma convection is controlled by ionospheric electric fields which are intimately connected with the magnetospheric-ionospheric current systems and are generally not readily modeled because of their complexity. There are a number of empirical models, however, which accurately model the overall convection patterns. We have made great progress adapting the convection model of Sojka et al.[9] to allow the FLIP model to include plasma drift. We are currently able to specify plasma trajectories as a function of time and interplanetary magnetic field strength and direction. The completion of the plasma convection algorithm will result in a much more accurate FLIP code in the auroral/polar regions.

3.4 Conductivity Calculations

A knowledge of ionospheric conductivities is central to an understanding of the coupled ionosphere-thermosphere-magnetosphere and the current systems flowing through them. Ionospheric conductivities arise from ionization due to both solar EUV illumination and incident particle flux. The combined FLIP and auroral codes provide local ionization densities from both sources. Thus we can calculate conductivities for a given set of model conditions. We have added such a calculation to the combined FLIP and auroral codes. In Figure 6 we show sample volume conductances due to an incident 5 kev auroral flux. (The model conditions have been chosen for local midnight in winter to minimize the EUV contributions.) Though the conductances peak in a narrow layer, the currents which flow through this region significantly influence plasma convection in the higher altitude regions.

We have extended the model to include a remotely measurable observable, FUV auroral emissions. Previously we demonstrated that selected ratios of OI 1356 Å and N_2 Lyman-Birge-Hopfield (LBH) emissions could be used to estimate the characteristic energy of

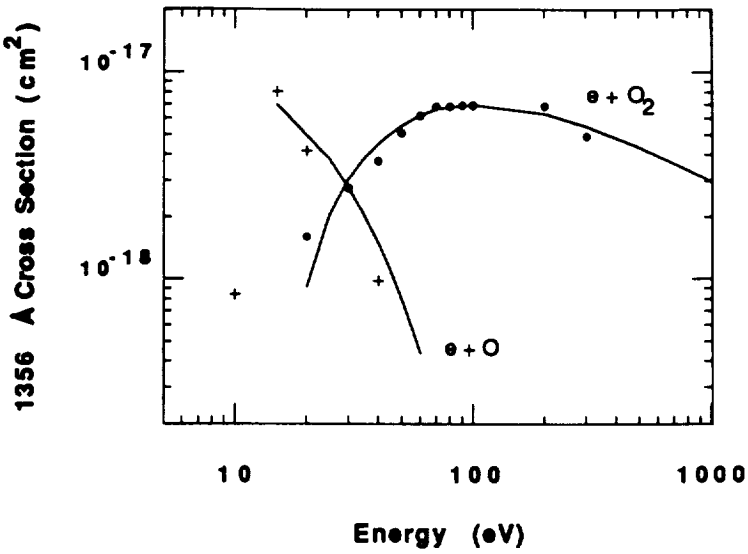

Figure 4

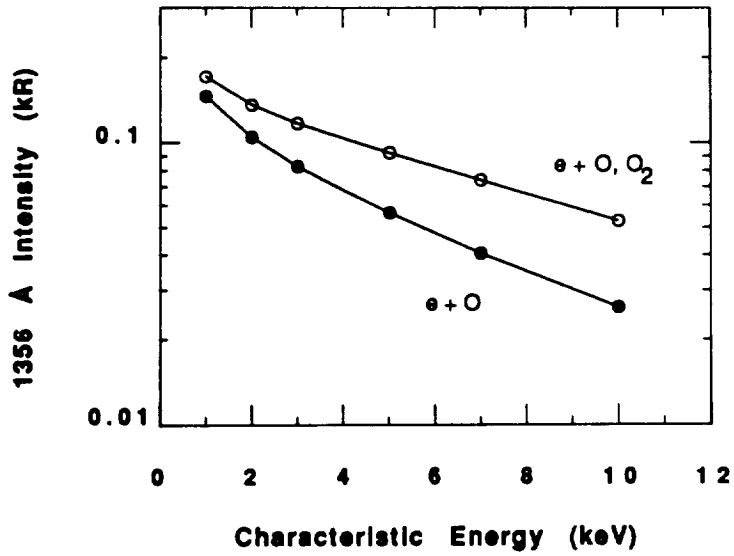

Figure 5

the precipitating electrons of a modeled aurora. This capability to remotely determine the incident electron energy can be coupled with the calculation of ionospheric conductances to provide a means of determining both the Pedersen and Hall column integrated ionospheric conductivities from measured FUV auroral emission intensity ratios. Figure 7 shows integrated column conductivities as a function of the ratio of two FUV auroral emissions (N_2 LBH 1838 Å and 1464 Å).

The relative paucity of experimental observations tends to limit the temporal and spatial scales of current conductivity models. Our combination of the conductivity calculation with a remotely measurable observable provides a valuable additional tool for increasing the number of experimental observations and, subsequently, our knowledge of the current systems in this region. Details of the conductivity calculation and its sensitivity to changes in characteristic energy, solar activity, and neutral composition were discussed at the Fall Meeting of the American Geophysical Union (December 12, 1991; San Francisco) by Dr. Germany.

3.5 UVI Workshops

We convened the second Ultraviolet Imager (UVI) workshop on August 1-2, 1991 in Salt Lake City, Utah. Like the first workshop, this meeting brought together nationally prominent scientists in the fields of ionospheric and magnetospheric physics and chemistry. The principal purpose of the workshop was to allow each of the attendees to participate in the mission science planning and to address their specific science requirements for the UVI instrument. The workshop participants and agenda are given in Table 1 of Appendix B - Semiannual Status Report. This workshop differed from the previous meeting in that the format was less structured and designed to encourage discussion among the participants. A large emphasis was given to defining and reviewing mission goals, to refining the models needed to attain these goals, and to implementing the goals in a practical manner.

Dr. Germany was responsible for coordination of the meeting. His responsibilities included arrangement of meeting facilities, communication with the science team members, and preparation of post workshop mailings. In addition, Dr. Germany participated in the workshop discussions and gave a presentation on the extraction of auroral parameters from auroral images via auroral modeling.

4. References

1. Donald F. Heath and Paul A. Sacher, Effects of a simulated high-energy space environment on the ultraviolet transmittance of optical materials between 1050 Å and 3000 Å, *Appl. Opt. 5*, 937, 1966.

2. C. A. Nicoletta and A. G. Eubanks, Effect of simulated space radiation on selected optical materials, *Appl. Opt. 11*, 1365, 1972.

3. C. S. Reft, J. Becher, and R. L. Kernell, Proton-induced degradation of VUV transmission of LiF and MgF_2, *Appl. Opt. 19*, 4156, 1980.

4. S. F. Pellicori, E. E. Russell, and L. A. Watts, Radiation induced transmission loss in optical materials, *Appl. Opt. 18*, 2618, 1979.

5. G. Hass and W. R. Hunter, Laboratory experiments to study surface contamination and degradation of optical coatings and materials in simulated space environments, *Appl. Opt. 9*, 2101, 1970.

6. Patrick N. Grillot and William J. Rosenberg, Proton radiation damage in optical filter glass, *Appl. Opt. 28*, 4473, 1989.

7. D. J. Strickland, R. R. Meier, J. H. Hecht, and A. B. Christensen, Deducing composition and incident electron spectra from ground-based auroral optical measurements: Theory and model results, *J. Geophys. Res. 94*, 13527, 1989.

8. W. C. Wells, W. L. Borst, and E. C. Zipf, Absolute cross section for the production of $O(^5S)$ by electron impact dissociation of O_2, *Chem. Phys. Lett. 12*, 288, 1971.

9. J. J. Sojka, C. E. Rasmussen, and R. W. Schunk, An interplanetary magnetic field dependent model of the ionospheric convection electric field, *J. Geophys. Res. 91*, 11281, 1986.

5. Appendix A - Radiation Test Results

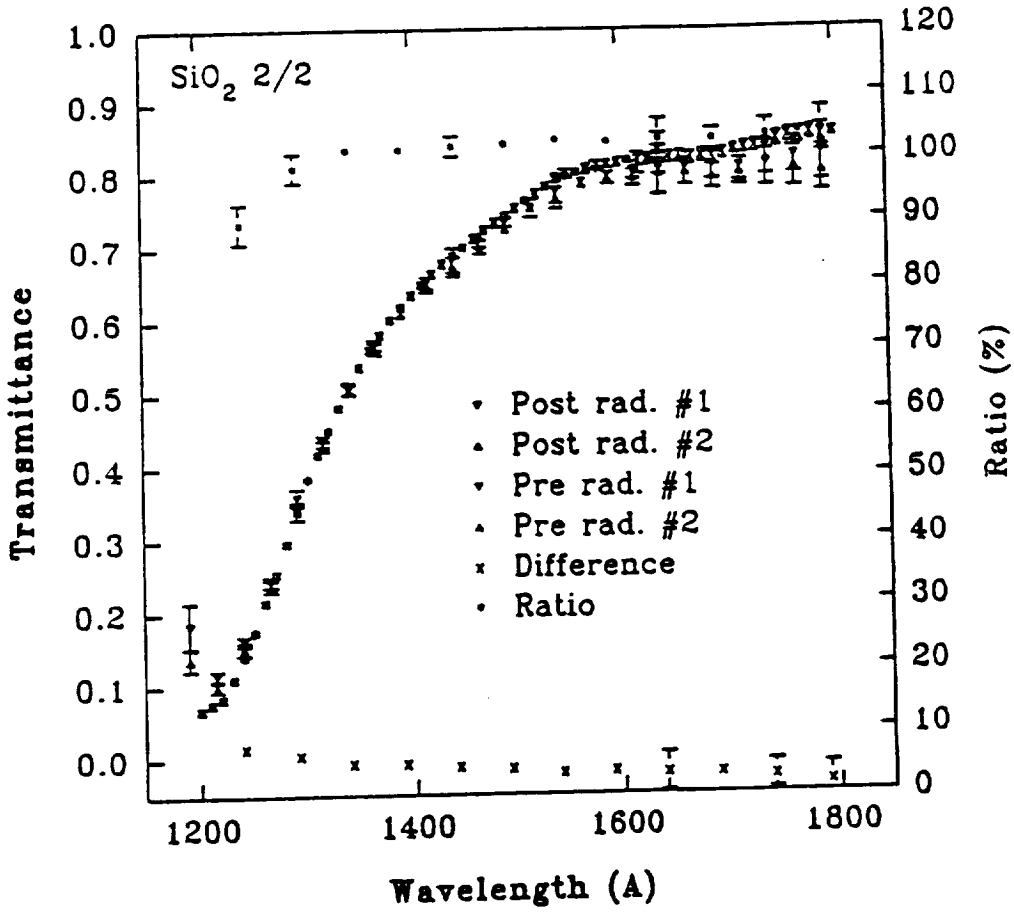
SiO2 2/2
Post rad. #1
Post rad. #2
Pre rad. #1
Pre rad. #2
Difference
Ratio
Transmittance
Ratio (%)
Wavelength (A)
1.0
0.9
0.8
0.7
0.6
0.5
0.4
0.3
0.2
0.1
0.0
120
110
100
90
80
70
60
50
40
30
20
10
0
1200
1400
1600
1800

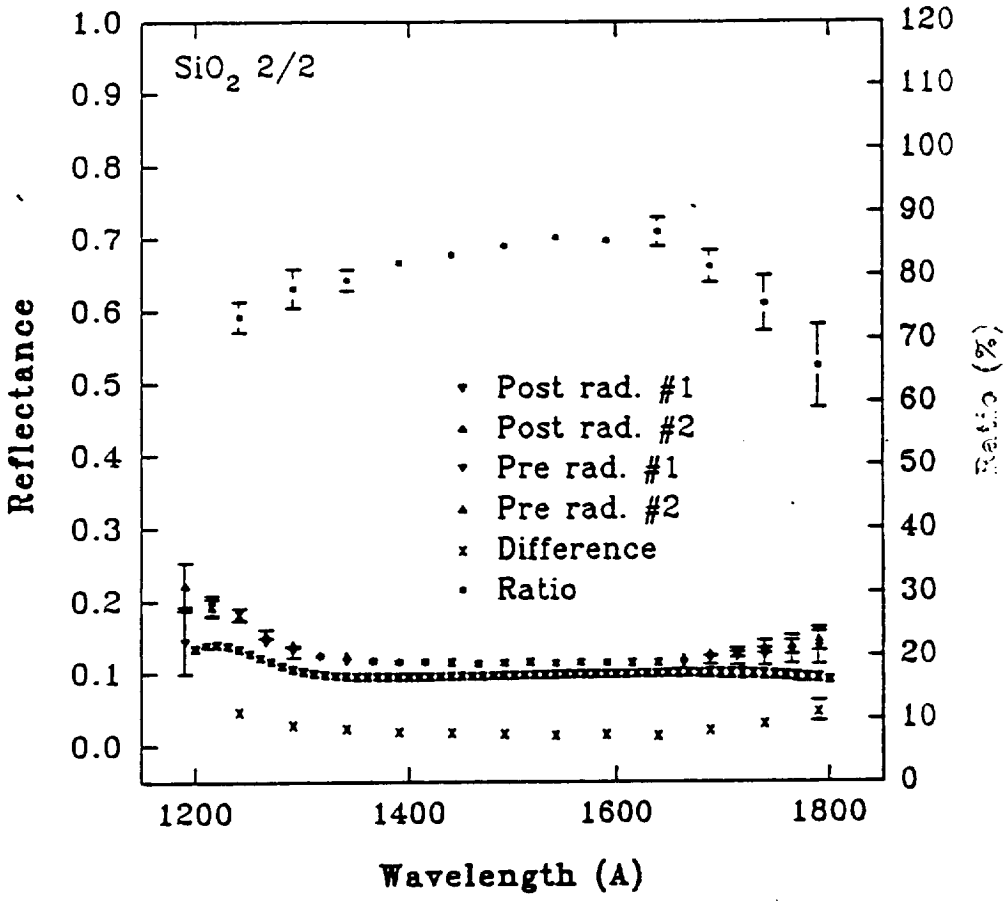
SiO2 2/2
Post rad. #1
Post rad. #2
Pre rad. #1
Pre rad. #2
Difference
Ratio
Reflectance
Ratio (%)
Wavelength (A)
1.0
0.9
0.8
0.7
0.6
0.5
0.4
0.3
0.2
0.1
0.0
120
110
100
90
80
70
60
50
40
30
20
10
0
1200
1400
1600
1800

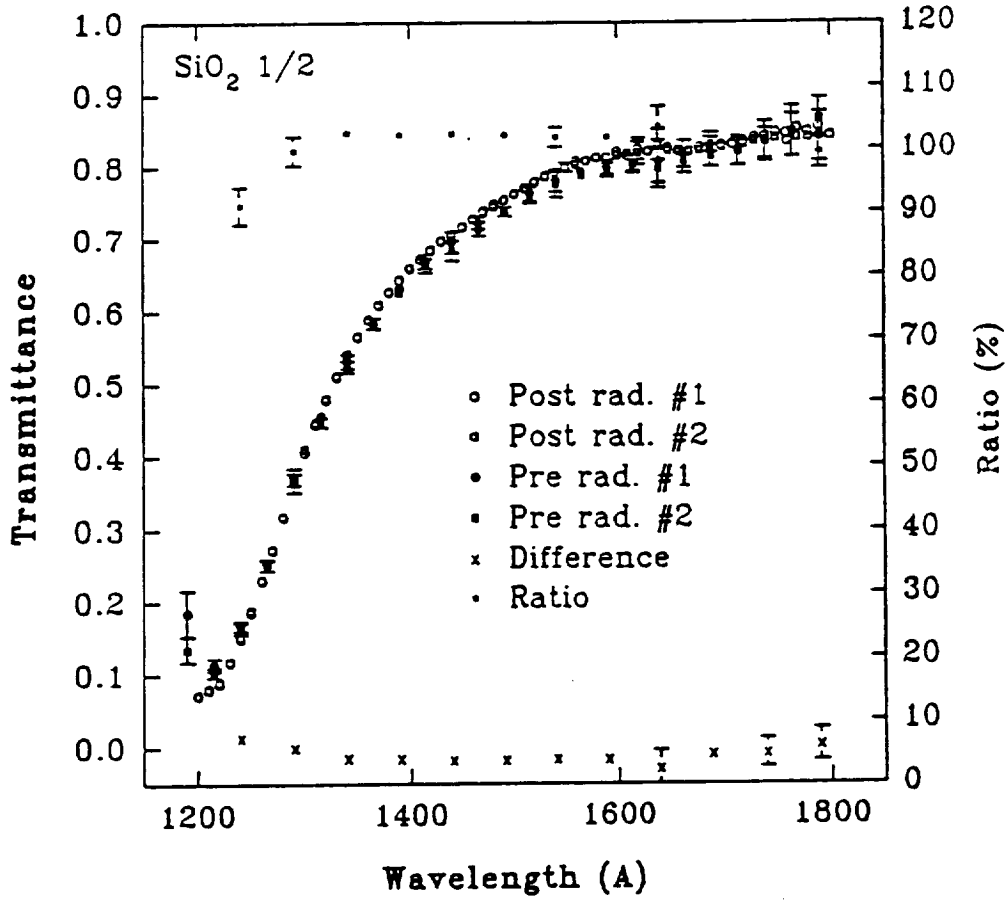
SiO2 1/2
Post rad. #1
Post rad. #2
Pre rad. #1
Pre rad. #2
Difference
Ratio
Transmittance
Ratio (%)
Wavelength (A)
1.0
0.9
0.8
0.7
0.6
0.5
0.4
0.3
0.2
0.1
0.0
120
110
100
90
80
70
60
50
40
30
20
10
0
1200
1400
1600
1800

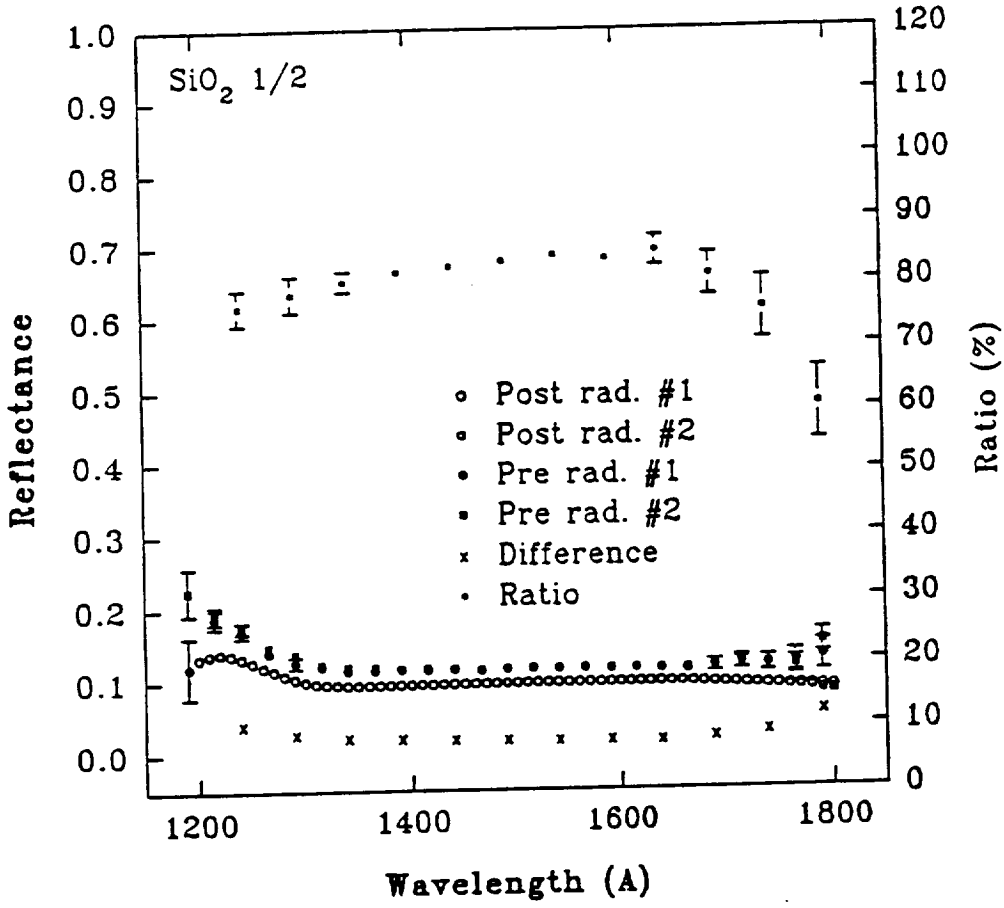
SiO2 1/2
Post rad. #1
Post rad. #2
Pre rad. #1
Pre rad. #2
Difference
Ratio
Reflectance
Ratio (%)
Wavelength (A)
1.0
0.9
0.8
0.7
0.6
0.5
0.4
0.3
0.2
0.1
0.0
120
110
100
90
80
70
60
50
40
30
20
10
0
1200
1400
1600
1800

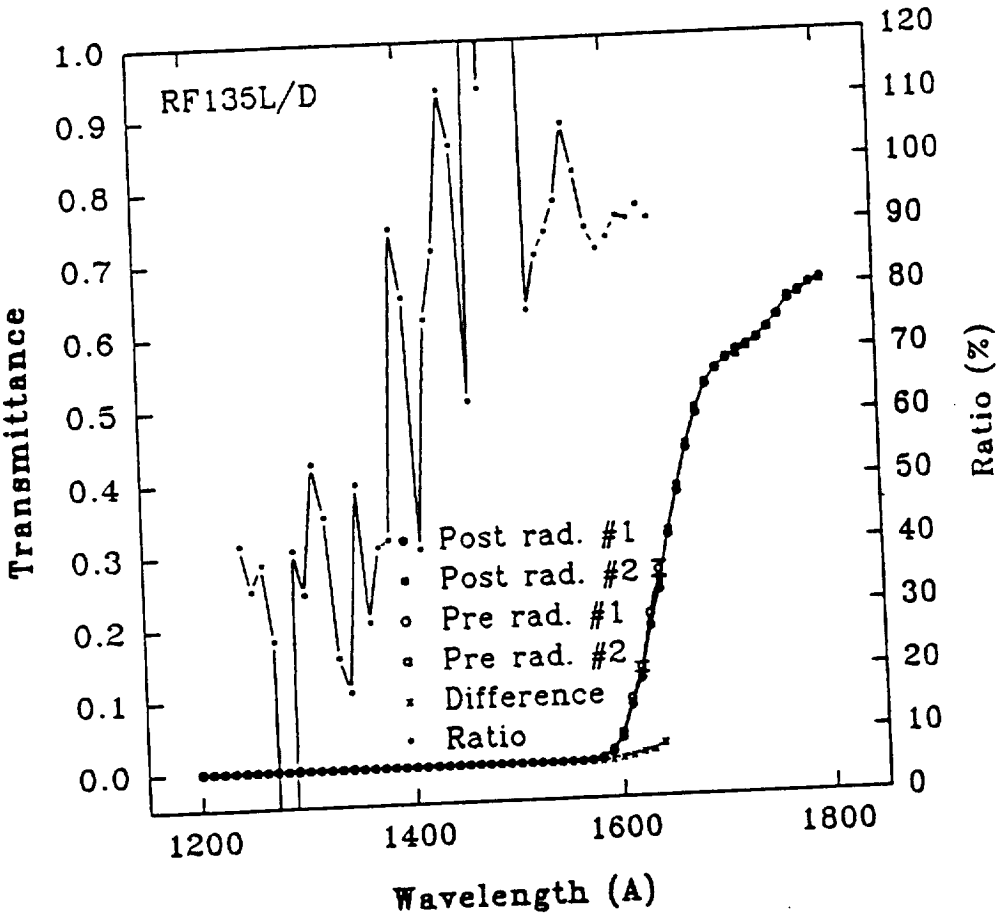
RF135L/D
Transmittance
Ratio (%)
Wavelength (A)
Post rad. #1
Post rad. #2
Pre rad. #1
Pre rad. #2
Difference
Ratio
1.0
0.9
0.8
0.7
0.6
0.5
0.4
0.3
0.2
0.1
0.0
120
110
100
90
80
70
60
50
40
30
20
10
0
1200
1400
1600
1800

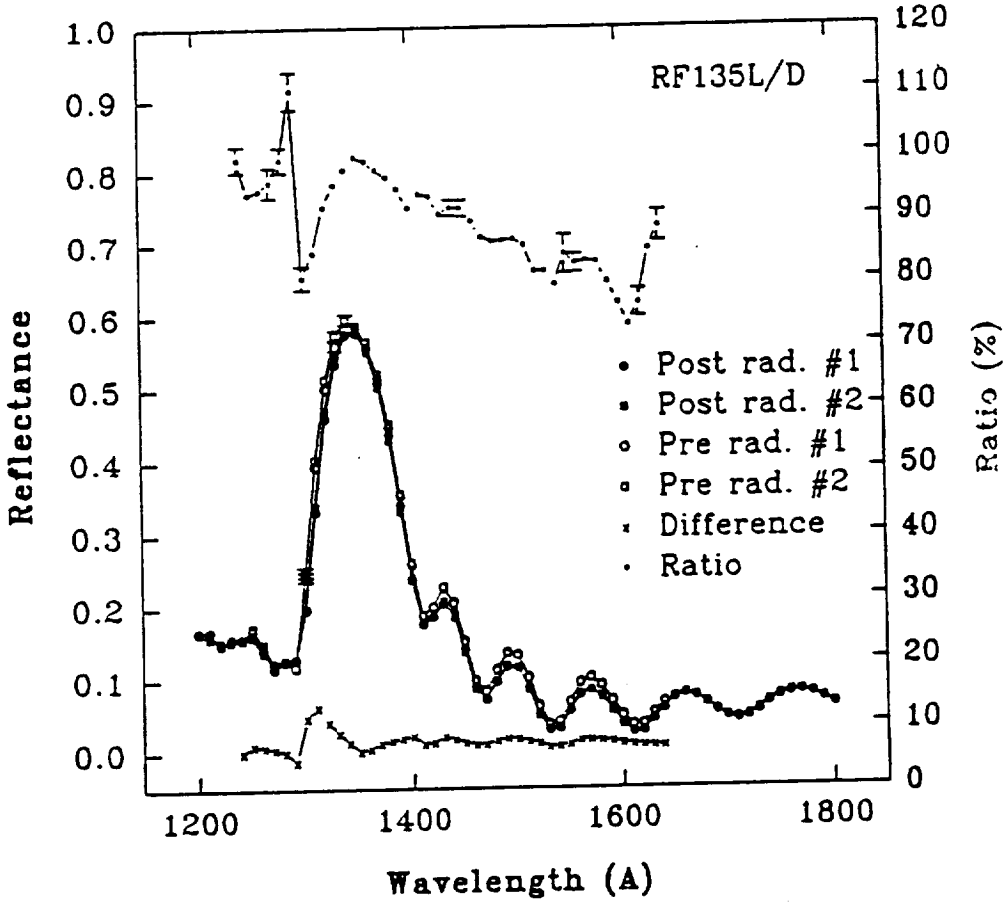
RF135L/D
Post rad. #1
Post rad. #2
Pre rad. #1
Pre rad. #2
Difference
Ratio
Reflectance
Ratio (%)
Wavelength (A)
1.0
0.9
0.8
0.7
0.6
0.5
0.4
0.3
0.2
0.1
0.0
120
110
100
90
80
70
60
50
40
30
20
10
0
1200
1400
1600
1800

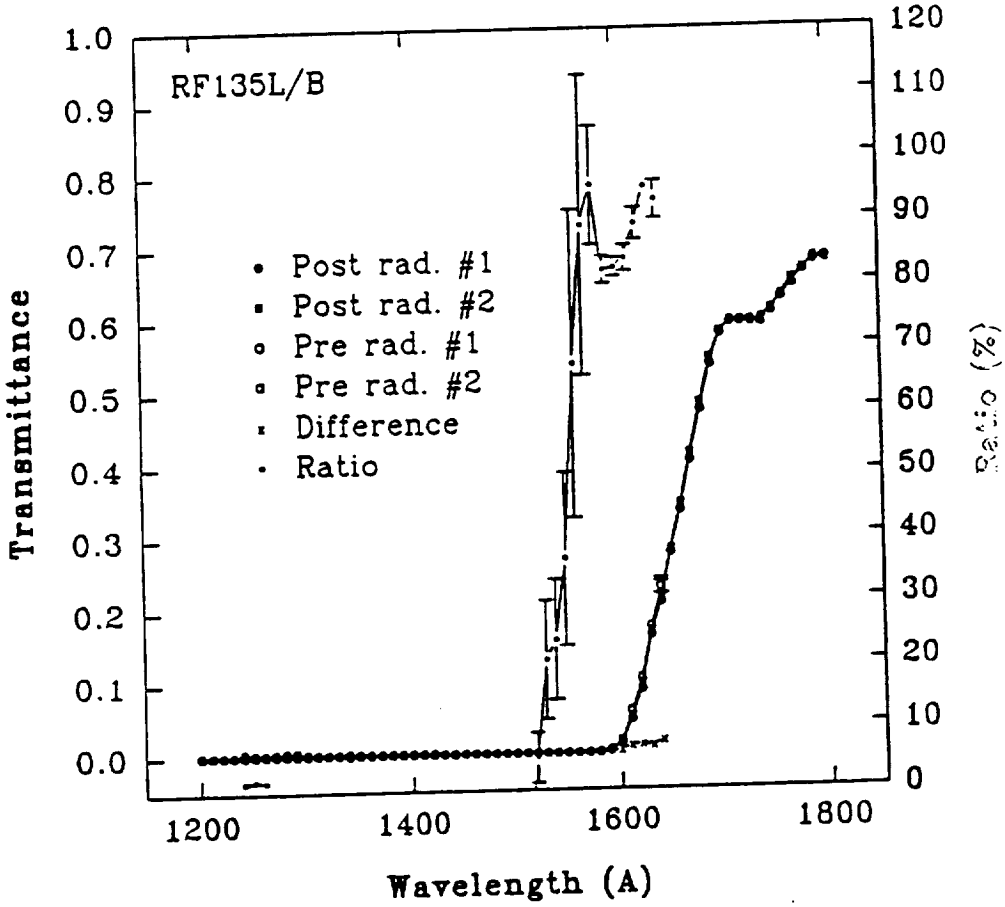
RF135L/B
Post rad. #1
Post rad. #2
Pre rad. #1
Pre rad. #2
Difference
Ratio
Transmittance
Wavelength (A)
Ratio (%)
1.0
0.9
0.8
0.7
0.6
0.5
0.4
0.3
0.2
0.1
0.0
120
110
100
90
80
70
60
50
40
30
20
10
0
1200
1400
1600
1800

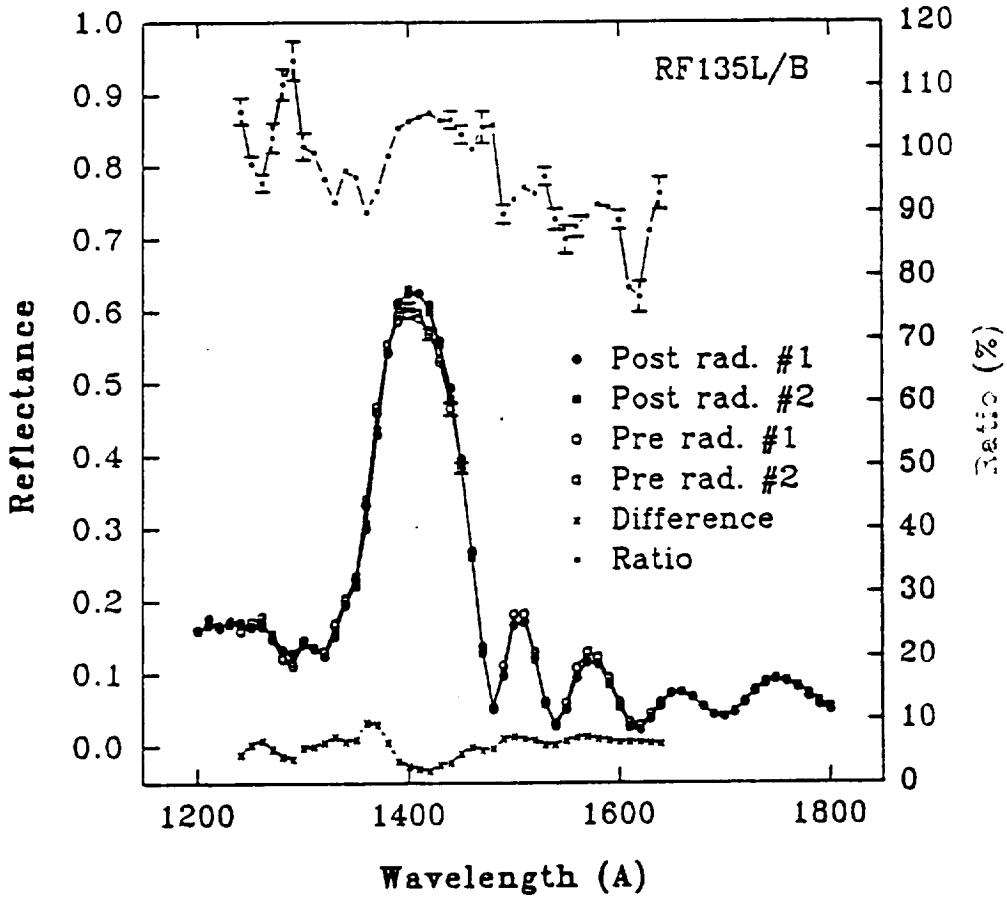
RF135L/B
Post rad. #1
Post rad. #2
Pre rad. #1
Pre rad. #2
Difference
Ratio
Reflectance
Ratio (%)
Wavelength (A)
1.0
0.9
0.8
0.7
0.6
0.5
0.4
0.3
0.2
0.1
0.0
120
110
100
90
80
70
60
50
40
30
20
10
0
1200
1400
1600
1800

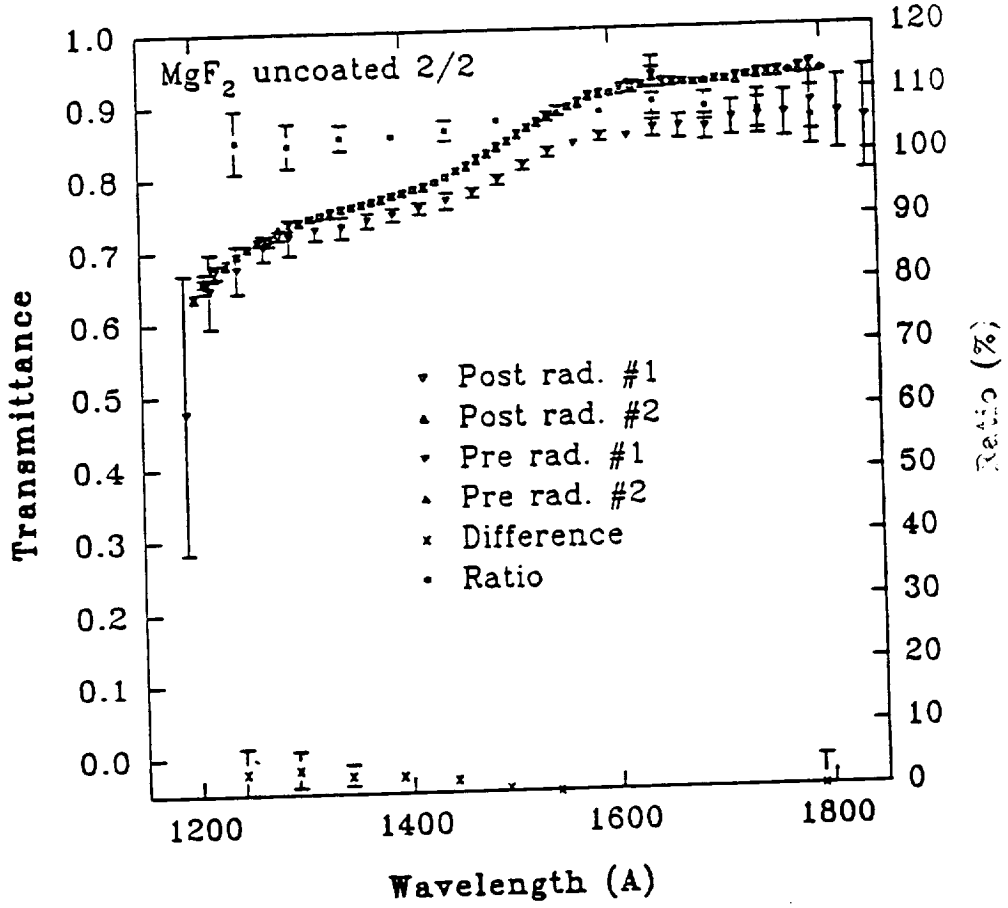
MgF2 uncoated 2/2
Post rad. #1
Post rad. #2
Pre rad. #1
Pre rad. #2
Difference
Ratio
Transmittance
Wavelength (A)
1.0
0.9
0.8
0.7
0.6
0.5
0.4
0.3
0.2
0.1
0.0
1200
1400
1600
1800
120
110
100
90
80
70
60
50
40
30
20
10
0

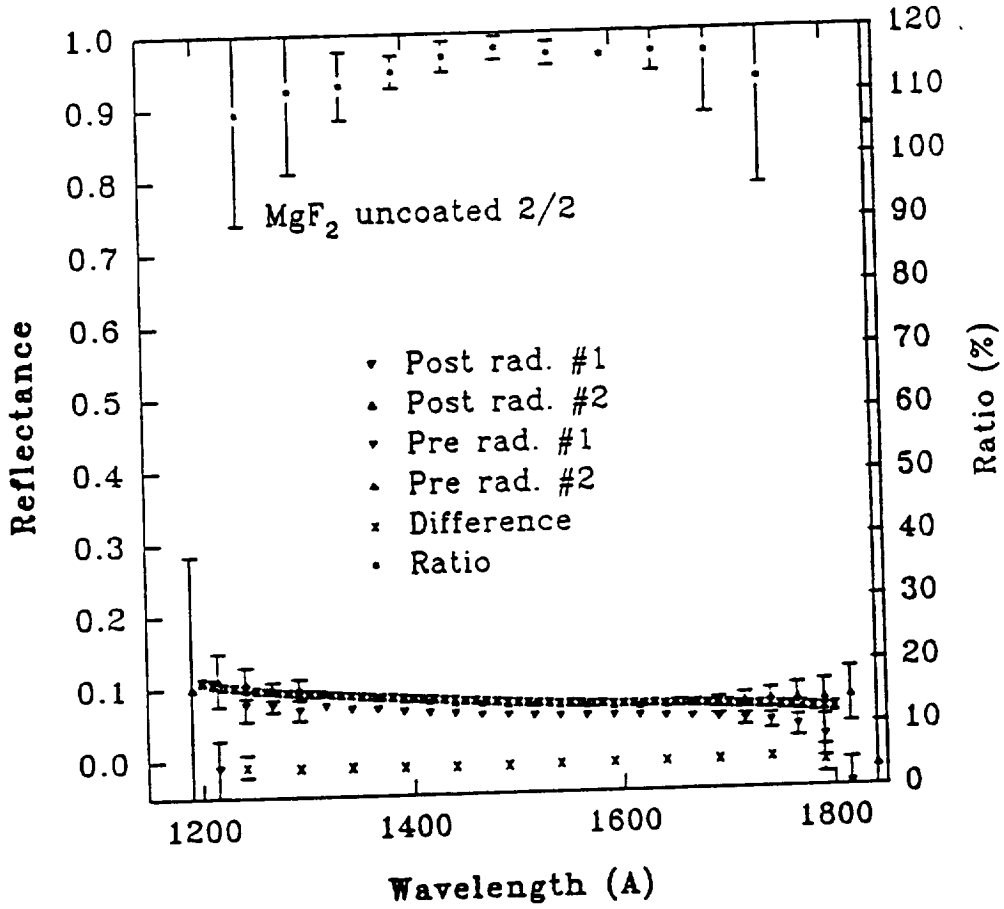
1.0
0.9
0.8
0.7
0.6
0.5
0.4
0.3
0.2
0.1
0.0
Reflectance
120
110
100
90
80
70
60
50
40
30
20
10
0
Ratio (%)
MgF2 uncoated 2/2
Post rad. #1
Post rad. #2
Pre rad. #1
Pre rad. #2
Difference
Ratio
1200
1400
1600
1800
Wavelength (A)

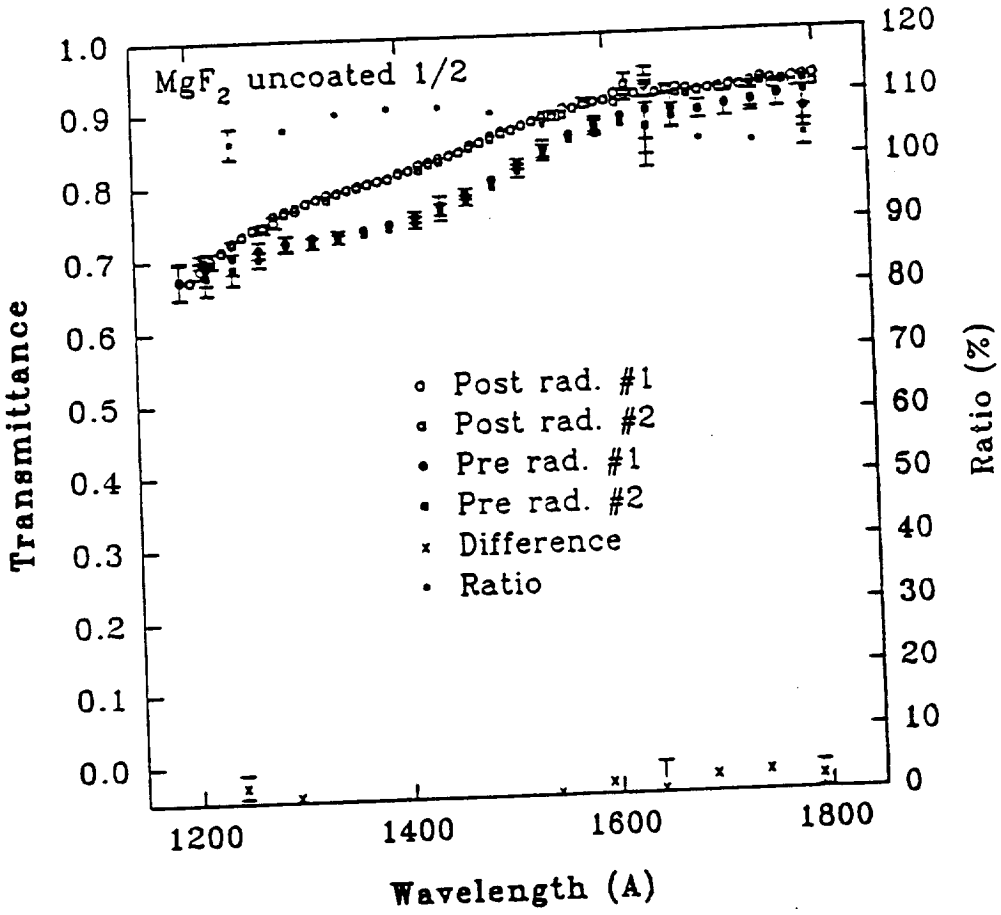
MgF2 uncoated 1/2
Post rad. #1
Post rad. #2
Pre rad. #1
Pre rad. #2
Difference
Ratio
Transmittance
Ratio (%)
Wavelength (A)
1.0
0.9
0.8
0.7
0.6
0.5
0.4
0.3
0.2
0.1
0.0
120
110
100
90
80
70
60
50
40
30
20
10
0
1200
1400
1600
1800

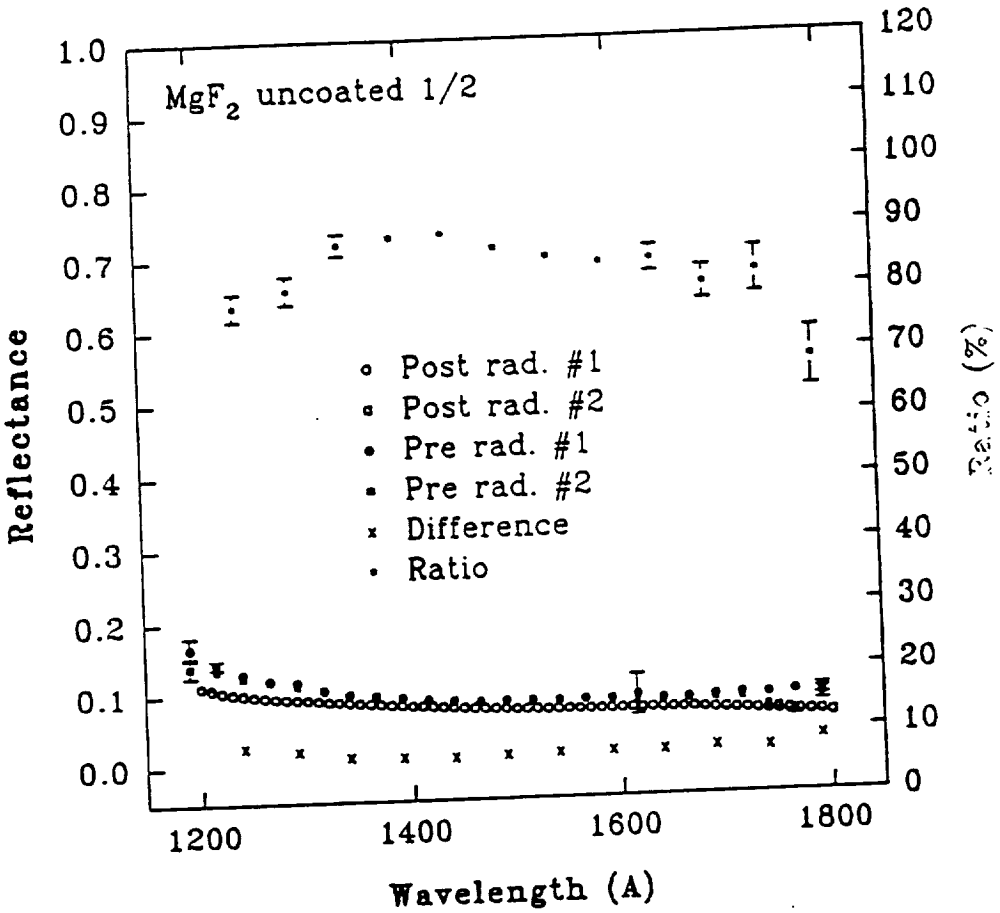
MgF2 uncoated 1/2
Post rad. #1
Post rad. #2
Pre rad. #1
Pre rad. #2
Difference
Ratio
Reflectance
Ratio (%)
Wavelength (A)
1.0
0.9
0.8
0.7
0.6
0.5
0.4
0.3
0.2
0.1
0.0
120
110
100
90
80
70
60
50
40
30
20
10
0
1200
1400
1600
1800

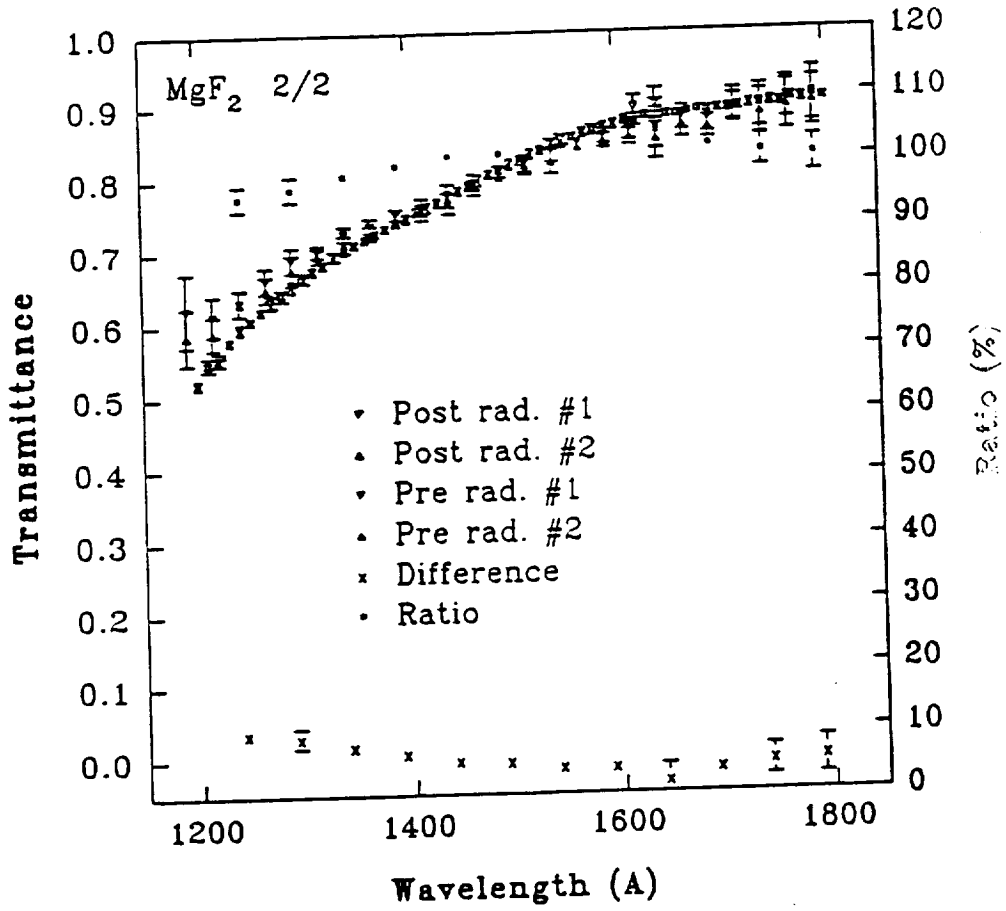
MgF2 2/2
Post rad. #1
Post rad. #2
Pre rad. #1
Pre rad. #2
Difference
Ratio
Transmittance
Wavelength (A)
Ratio (%)
1.0
0.9
0.8
0.7
0.6
0.5
0.4
0.3
0.2
0.1
0.0
120
110
100
90
80
70
60
50
40
30
20
10
0
1200
1400
1600
1800

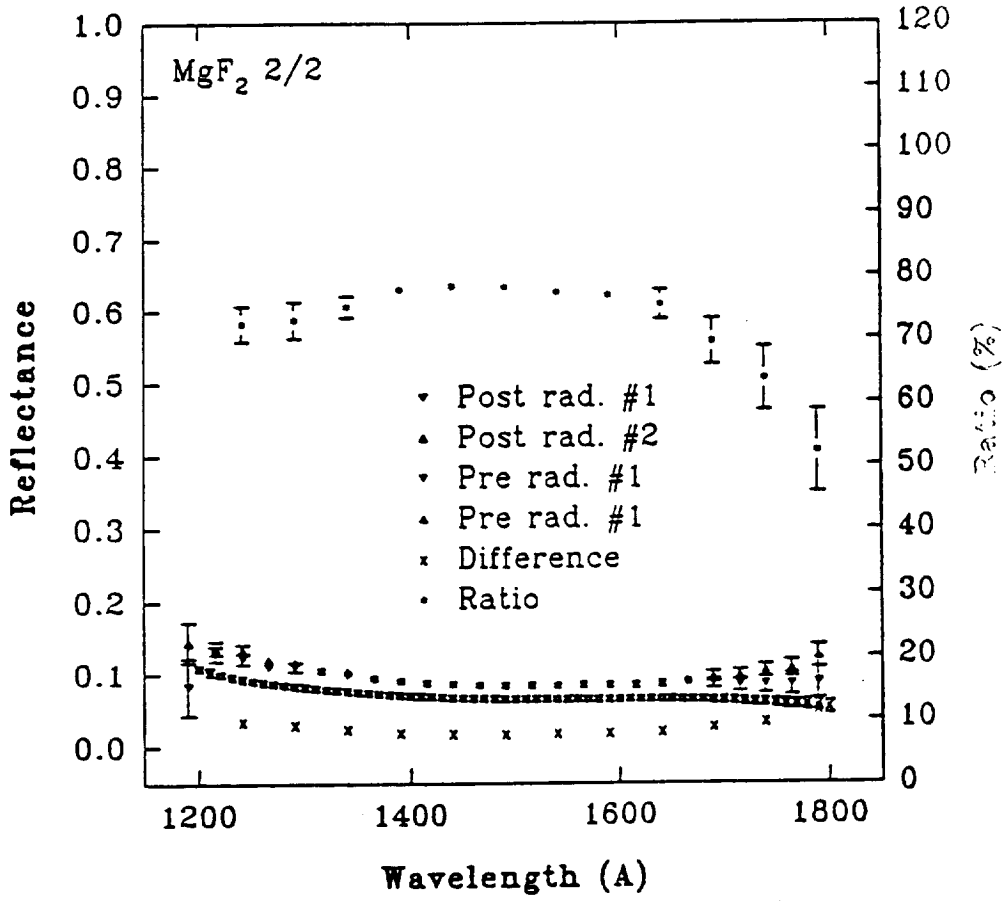
MgF2 2/2
Post rad. #1
Post rad. #2
Pre rad. #1
Pre rad. #1
Difference
Ratio
Reflectance
Wavelength (A)
1.0
0.9
0.8
0.7
0.6
0.5
0.4
0.3
0.2
0.1
0.0
120
110
100
90
80
70
60
50
40
30
20
10
0
1200
1400
1600
1800

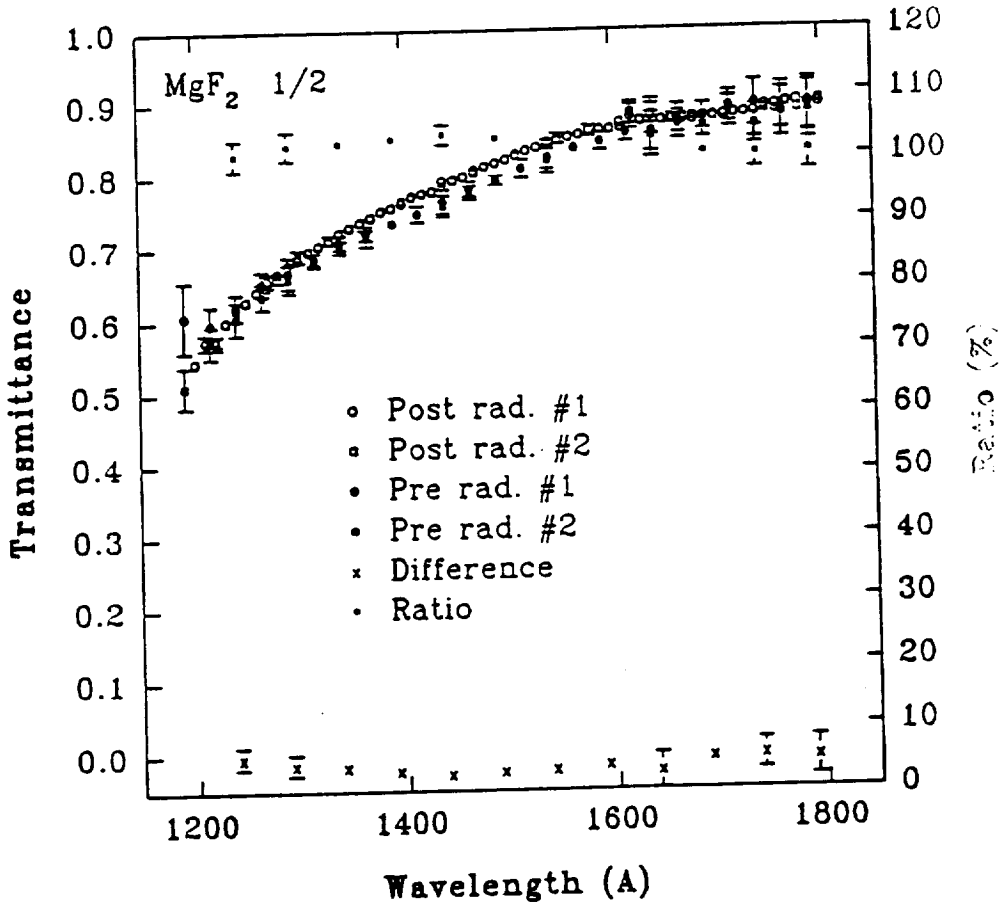
MgF2 1/2
Post rad. #1
Post rad. #2
Pre rad. #1
Pre rad. #2
Difference
Ratio
Transmittance
Ratio (%)
Wavelength (A)
1.0
0.9
0.8
0.7
0.6
0.5
0.4
0.3
0.2
0.1
0.0
120
110
100
90
80
70
60
50
40
30
20
10
0
1200
1400
1600
1800

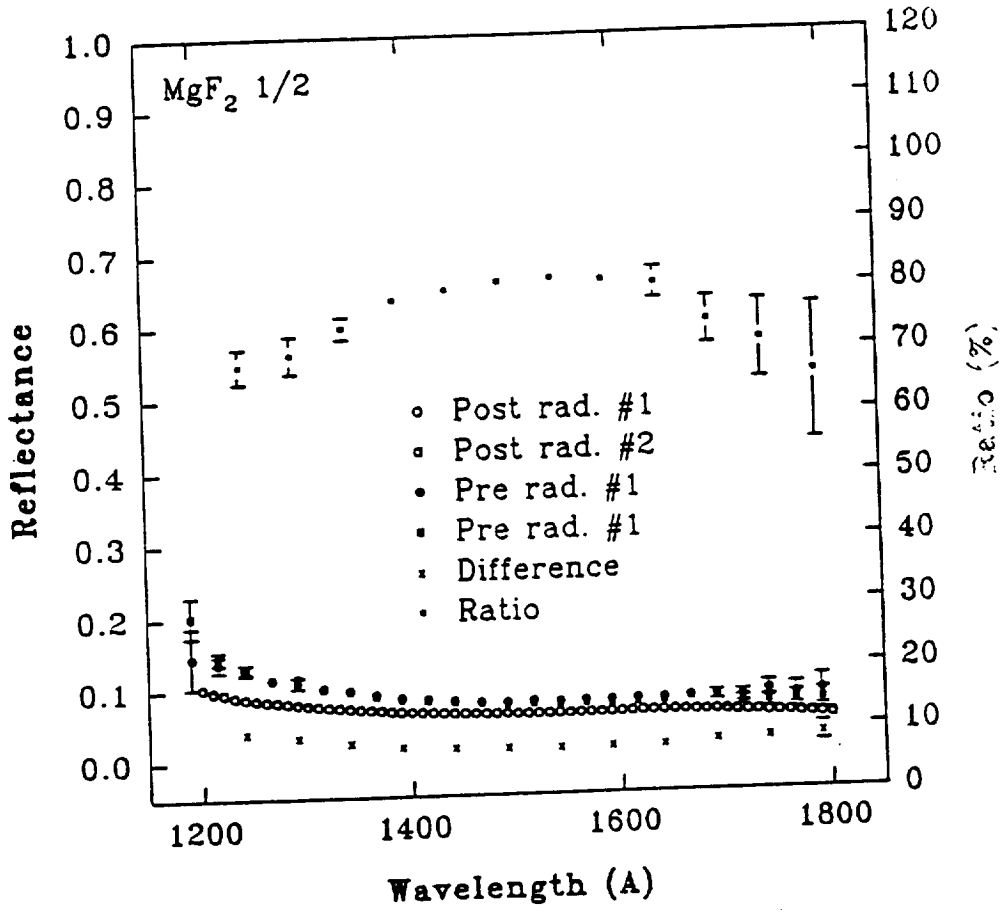
MgF2 1/2
Post rad. #1
Post rad. #2
Pre rad. #1
Pre rad. #1
Difference
Ratio
Reflectance
Wavelength (A)
1.0
0.9
0.8
0.7
0.6
0.5
0.4
0.3
0.2
0.1
0.0
120
110
100
90
80
70
60
50
40
30
20
10
0
1200
1400
1600
1800

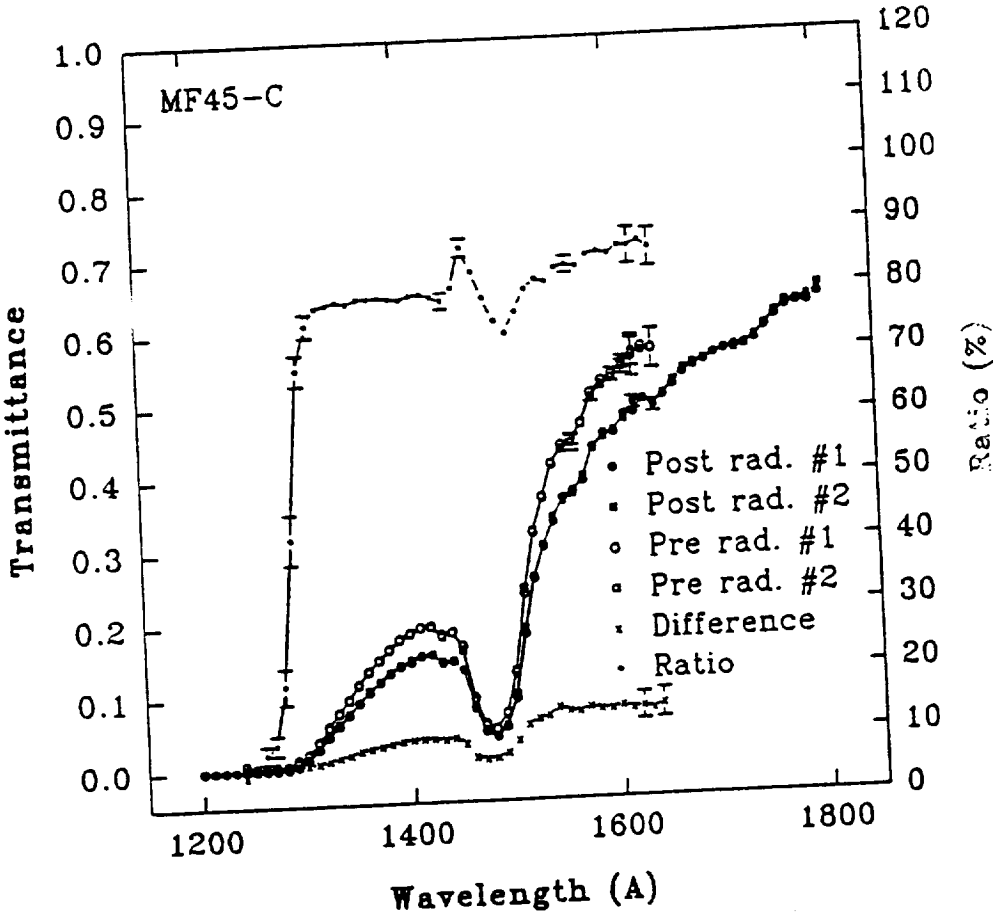
MF45-C
Transmittance
Wavelength (A)
Ratio (%)
Post rad. #1
Post rad. #2
Pre rad. #1
Pre rad. #2
Difference
Ratio
1.0
0.9
0.8
0.7
0.6
0.5
0.4
0.3
0.2
0.1
0.0
120
110
100
90
80
70
60
50
40
30
20
10
0
1200
1400
1600
1800

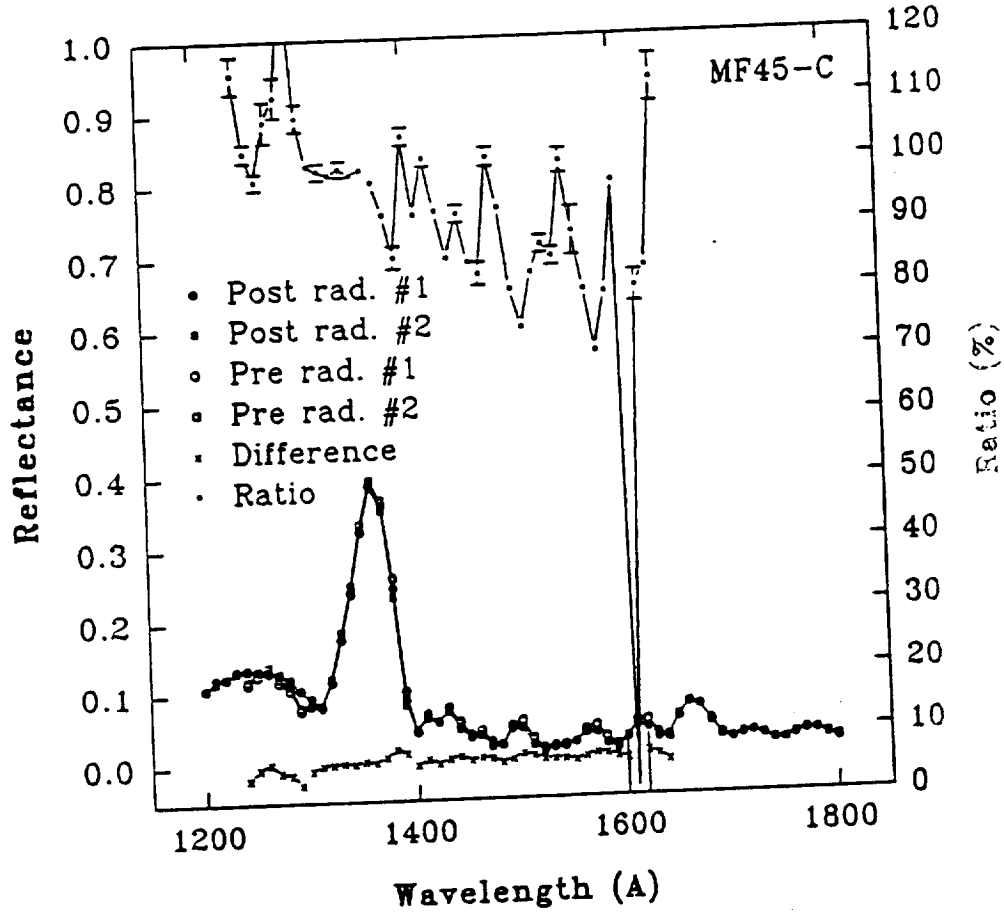
MF45-C
Post rad. #1
Post rad. #2
Pre rad. #1
Pre rad. #2
Difference
Ratio
Reflectance
Ratio (%)
Wavelength (A)
1.0
0.9
0.8
0.7
0.6
0.5
0.4
0.3
0.2
0.1
0.0
120
110
100
90
80
70
60
50
40
30
20
10
0
1200
1400
1600
1800

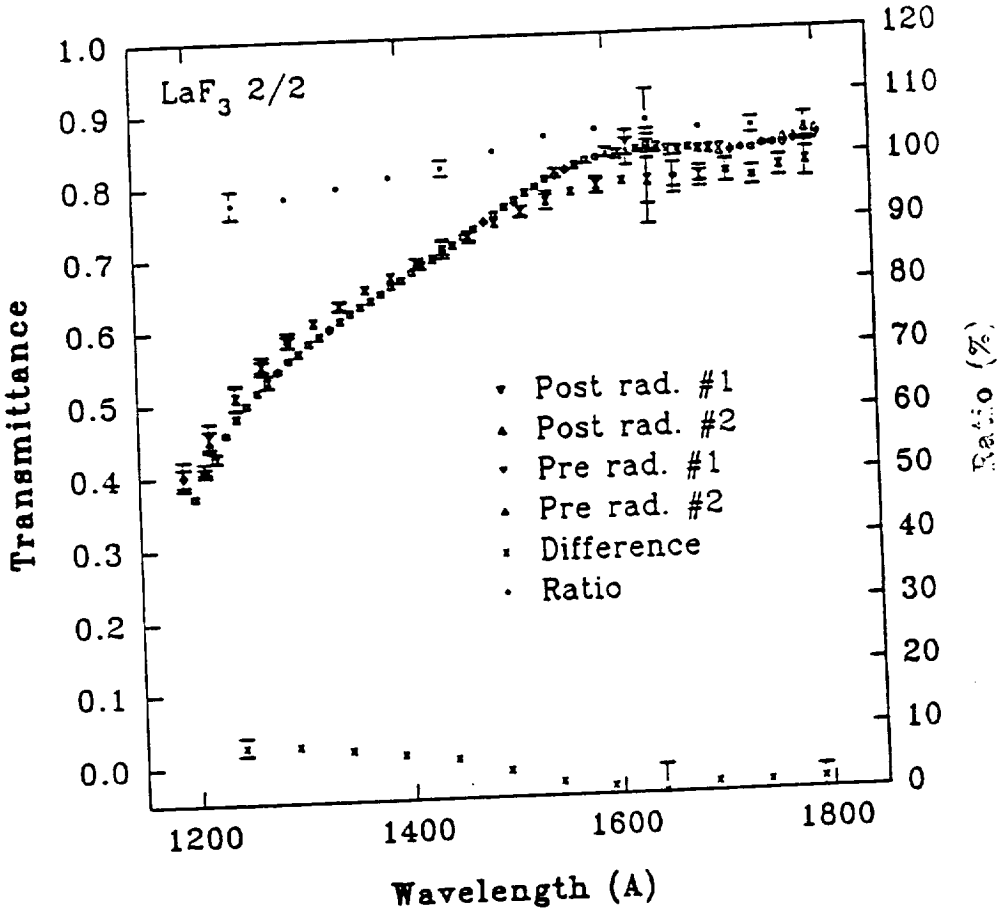
LaF3 2/2
Transmittance
Wavelength (A)
Ratio (%)
Post rad. #1
Post rad. #2
Pre rad. #1
Pre rad. #2
Difference
Ratio
1.0
0.9
0.8
0.7
0.6
0.5
0.4
0.3
0.2
0.1
0.0
120
110
100
90
80
70
60
50
40
30
20
10
0
1200
1400
1600
1800

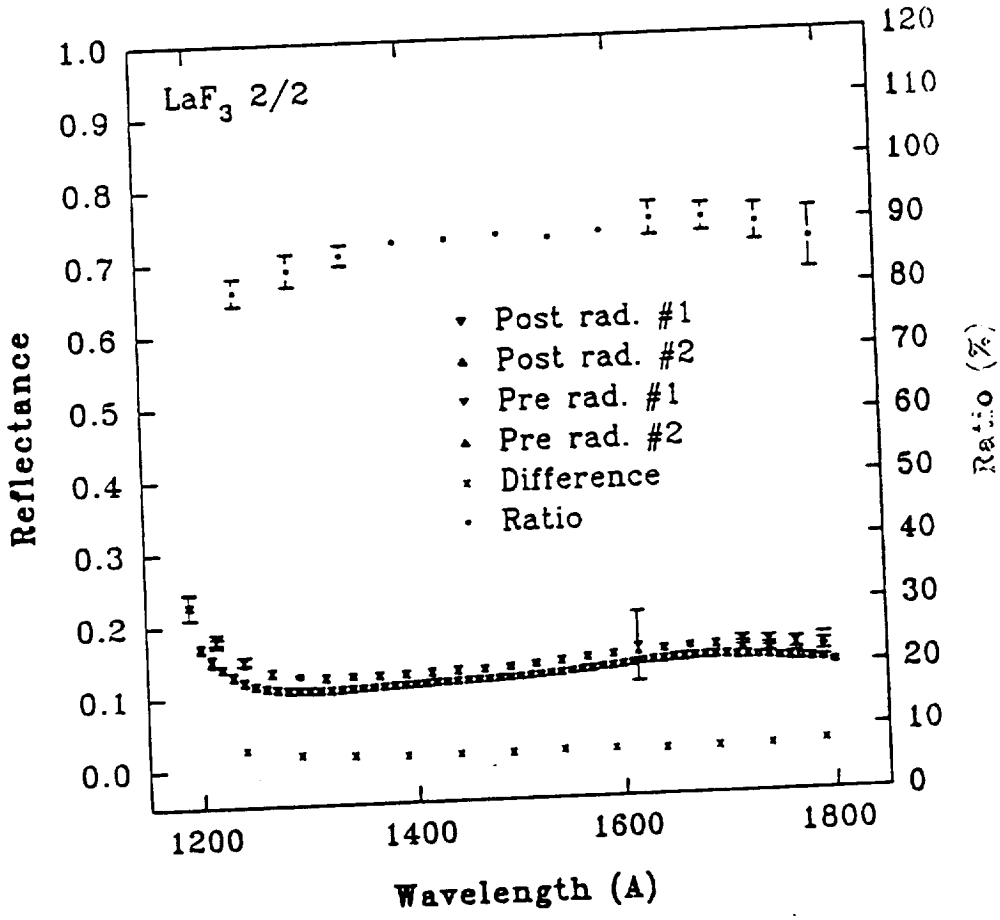
LaF3 2/2
Post rad. #1
Post rad. #2
Pre rad. #1
Pre rad. #2
Difference
Ratio
Reflectance
Ratio (%)
Wavelength (A)
1.0
0.9
0.8
0.7
0.6
0.5
0.4
0.3
0.2
0.1
0.0
120
110
100
90
80
70
60
50
40
30
20
10
0
1200
1400
1600
1800

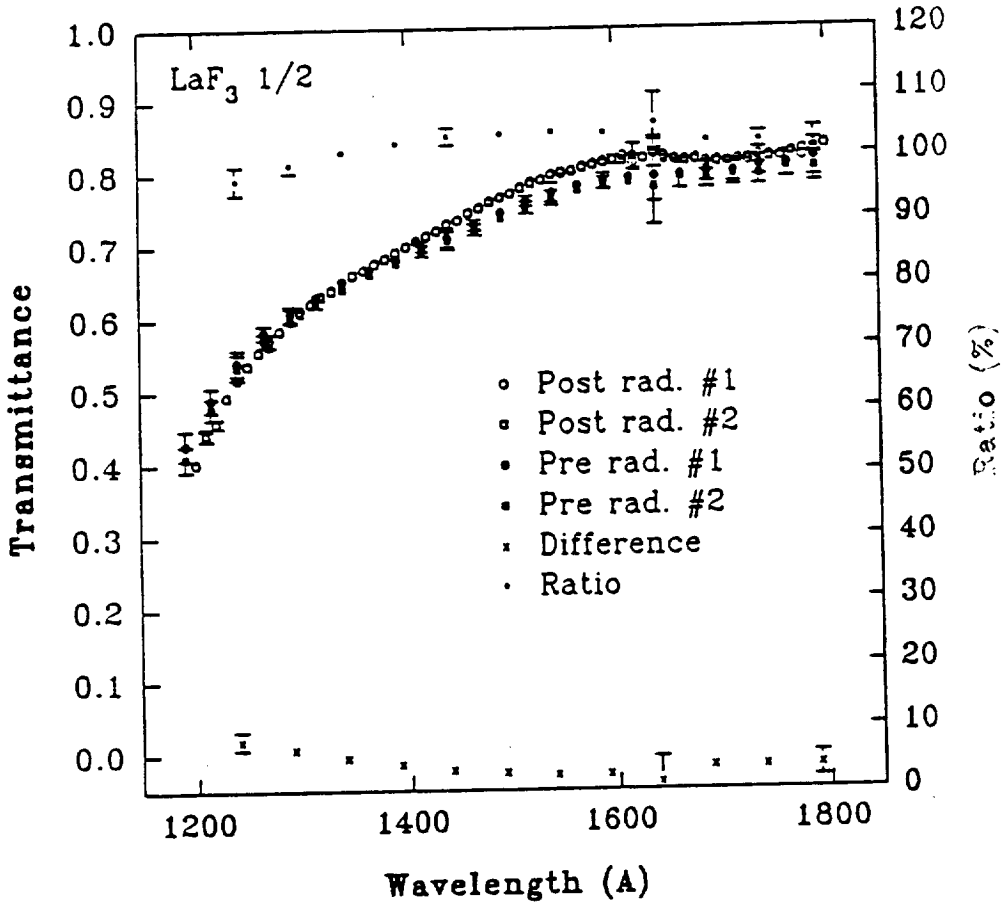
LaF3 1/2
Post rad. #1
Post rad. #2
Pre rad. #1
Pre rad. #2
Difference
Ratio
Transmittance
Ratio (%)
Wavelength (A)
1.0
0.9
0.8
0.7
0.6
0.5
0.4
0.3
0.2
0.1
0.0
120
110
100
90
80
70
60
50
40
30
20
10
0
1200
1400
1600
1800

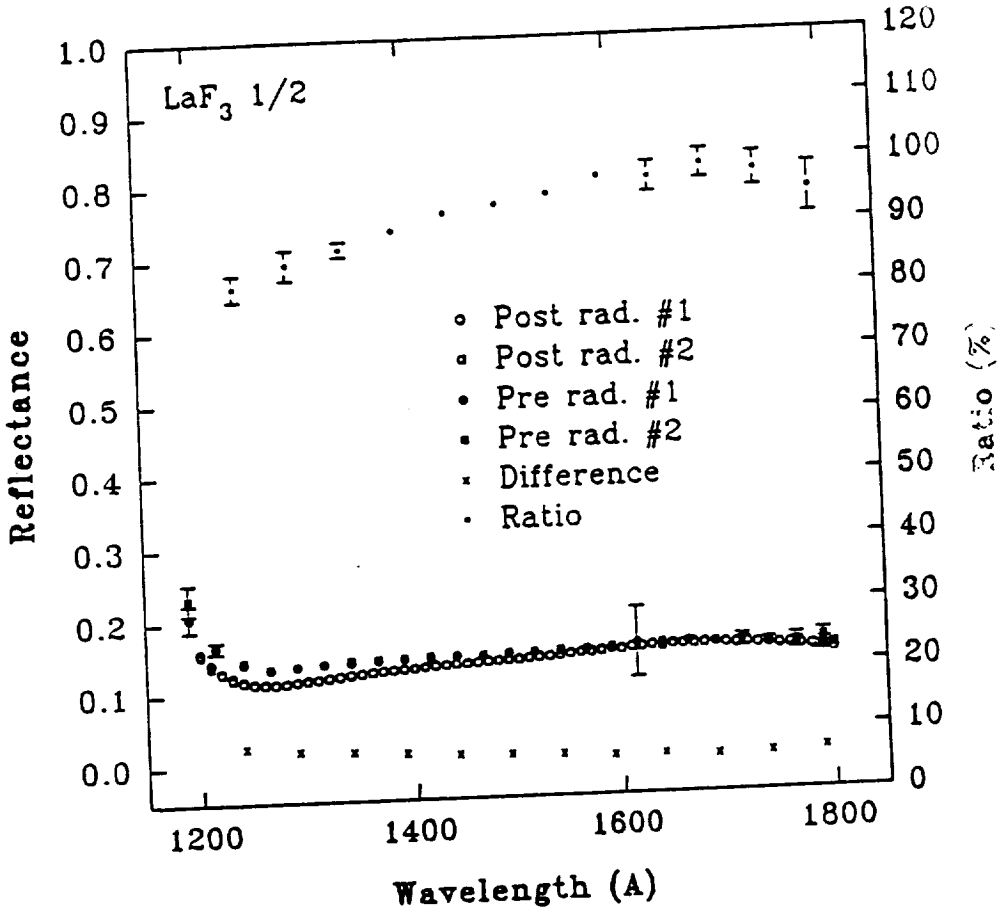
LaF3 1/2
Post rad. #1
Post rad. #2
Pre rad. #1
Pre rad. #2
Difference
Ratio
Reflectance
Ratio (%)
Wavelength (A)
1.0
0.9
0.8
0.7
0.6
0.5
0.4
0.3
0.2
0.1
0.0
120
110
100
90
80
70
60
50
40
30
20
10
0
1200
1400
1600
1800

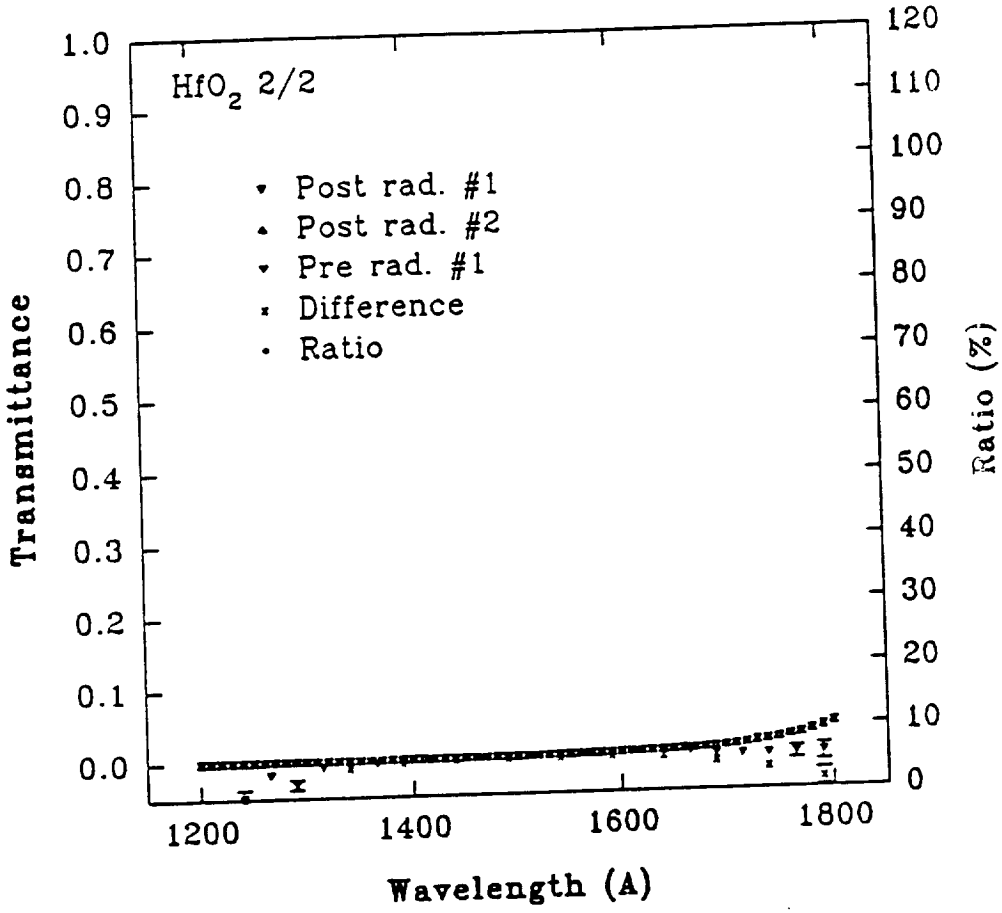
HfO2 2/2
Post rad. #1
Post rad. #2
Pre rad. #1
Difference
Ratio
Transmittance
Ratio (%)
Wavelength (A)
1.0
0.9
0.8
0.7
0.6
0.5
0.4
0.3
0.2
0.1
0.0
120
110
100
90
80
70
60
50
40
30
20
10
0
1200
1400
1600
1800

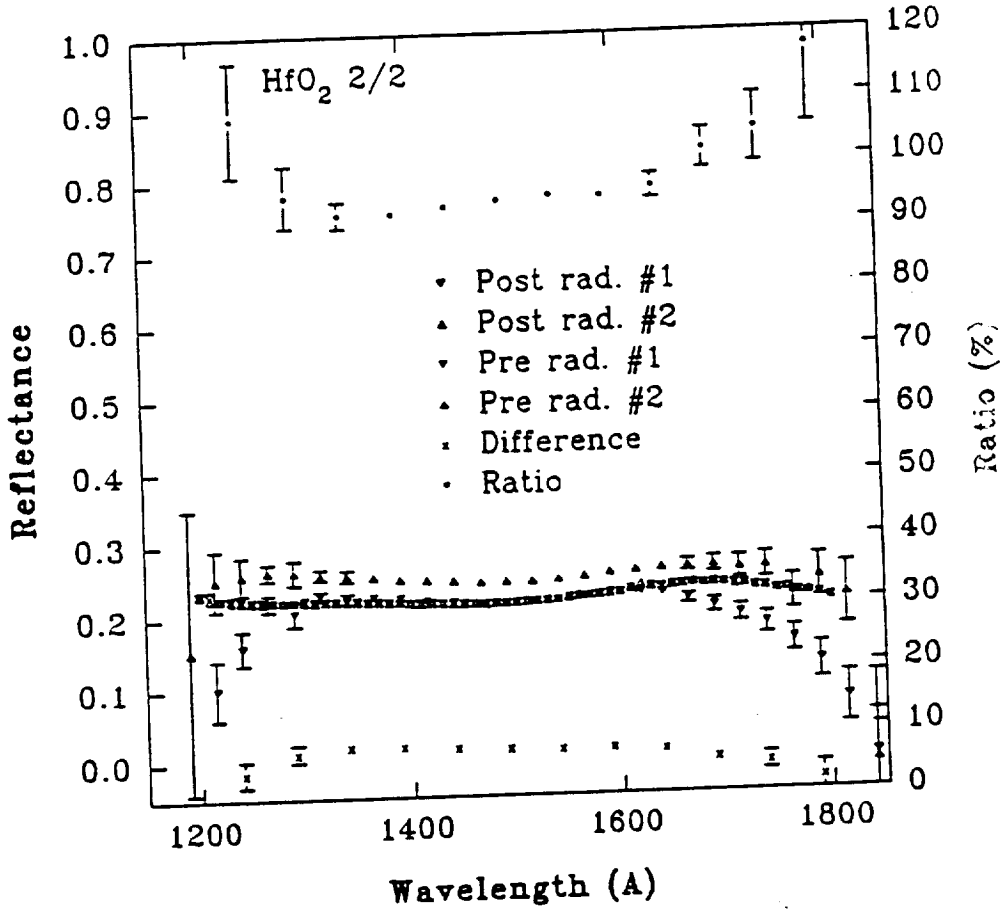
HfO2 2/2
Post rad. #1
Post rad. #2
Pre rad. #1
Pre rad. #2
Difference
Ratio
Reflectance
Ratio (%)
Wavelength (A)
1.0
0.9
0.8
0.7
0.6
0.5
0.4
0.3
0.2
0.1
0.0
120
110
100
90
80
70
60
50
40
30
20
10
0
1200
1400
1600
1800

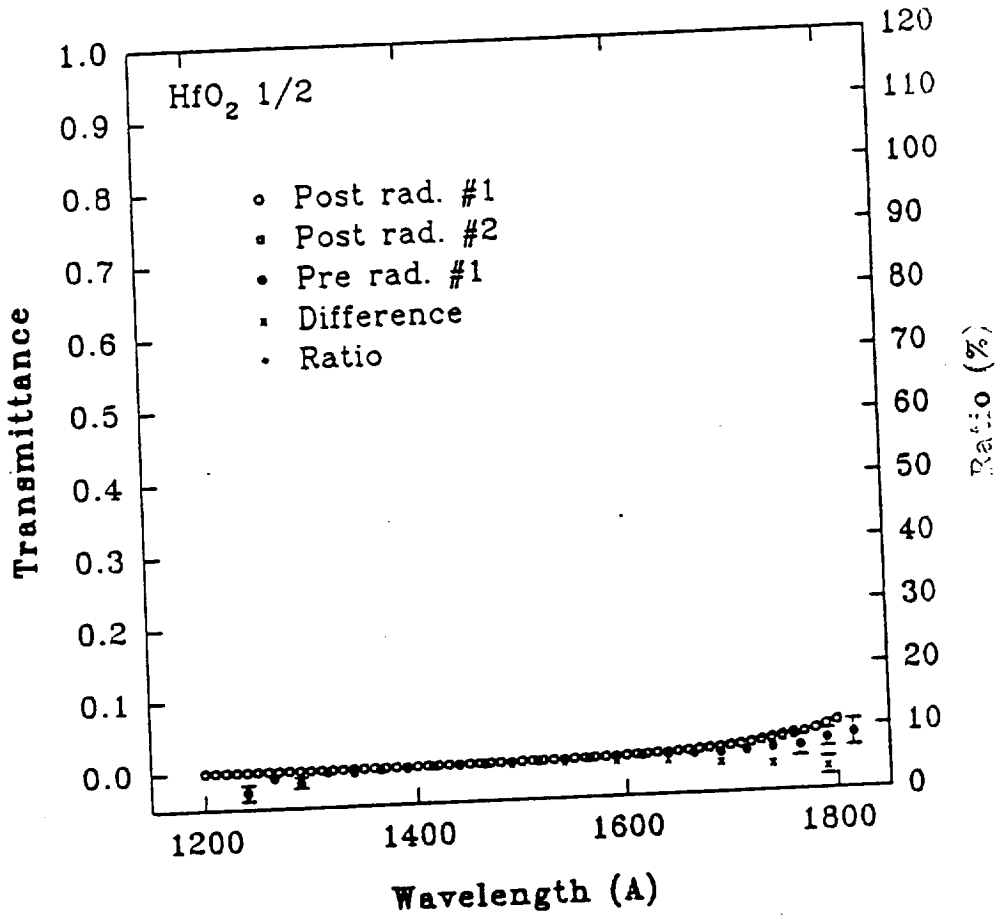
HfO_2 1/2
Post rad. #1
Post rad. #2
Pre rad. #1
Difference
Ratio
Transmittance
Ratio (%)
Wavelength (A)
1.0
0.9
0.8
0.7
0.6
0.5
0.4
0.3
0.2
0.1
0.0
120
110
100
90
80
70
60
50
40
30
20
10
0
1200
1400
1600
1800

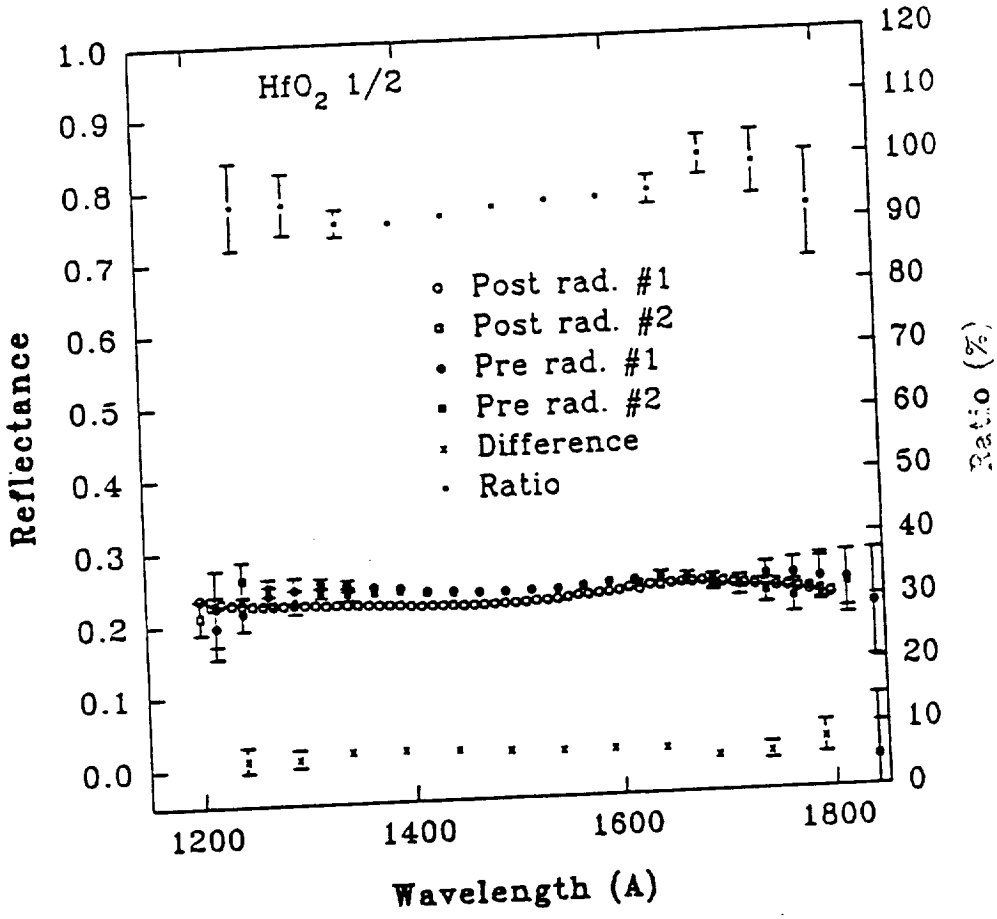
HfO2 1/2
Post rad. #1
Post rad. #2
Pre rad. #1
Pre rad. #2
Difference
Ratio
Reflectance
Ratio (%)
Wavelength (A)
1.0
0.9
0.8
0.7
0.6
0.5
0.4
0.3
0.2
0.1
0.0
120
110
100
90
80
70
60
50
40
30
20
10
0
1200
1400
1600
1800

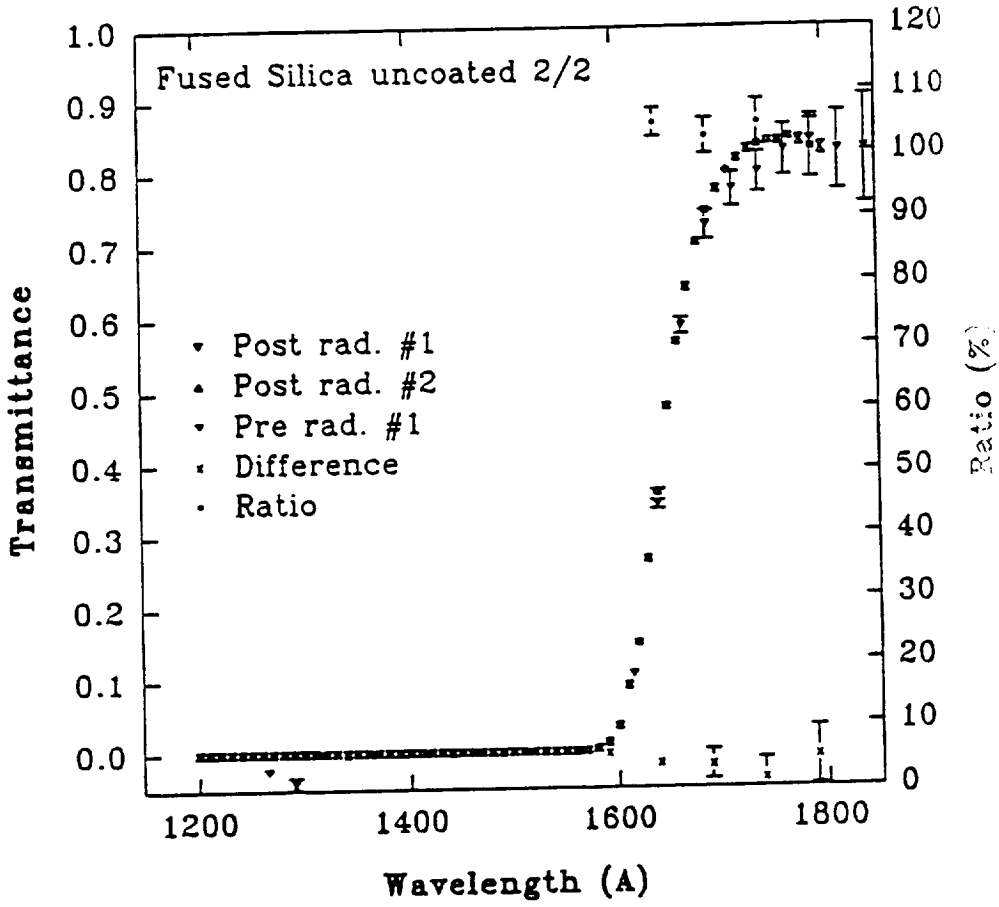
Fused Silica uncoated 2/2
Post rad. #1
Post rad. #2
Pre rad. #1
Difference
Ratio
Transmittance
Ratio (%)
Wavelength (A)
1.0
0.9
0.8
0.7
0.6
0.5
0.4
0.3
0.2
0.1
0.0
120
110
100
90
80
70
60
50
40
30
20
10
0
1200
1400
1600
1800

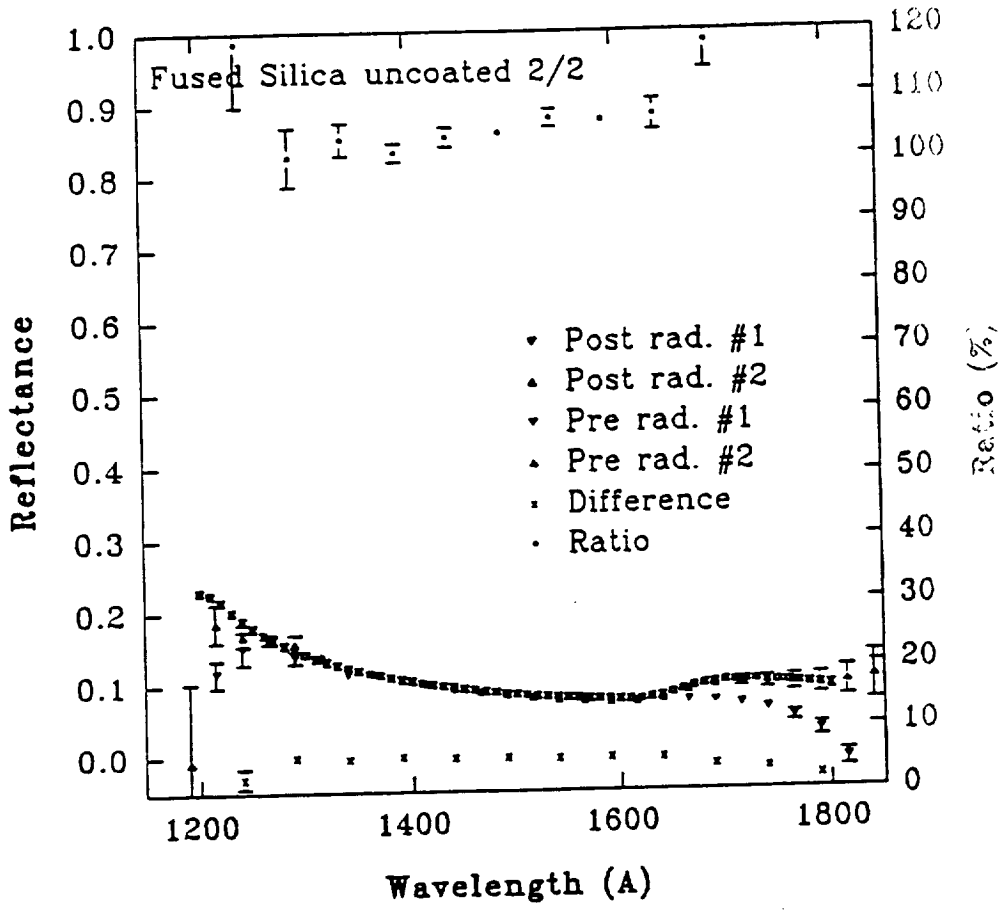
Fused Silica uncoated 2/2
Post rad. #1
Post rad. #2
Pre rad. #1
Pre rad. #2
Difference
Ratio
Reflectance
Wavelength (A)
1.0
0.9
0.8
0.7
0.6
0.5
0.4
0.3
0.2
0.1
0.0
1200
1400
1600
1800
120
110
100
90
80
70
60
50
40
30
20
10
0

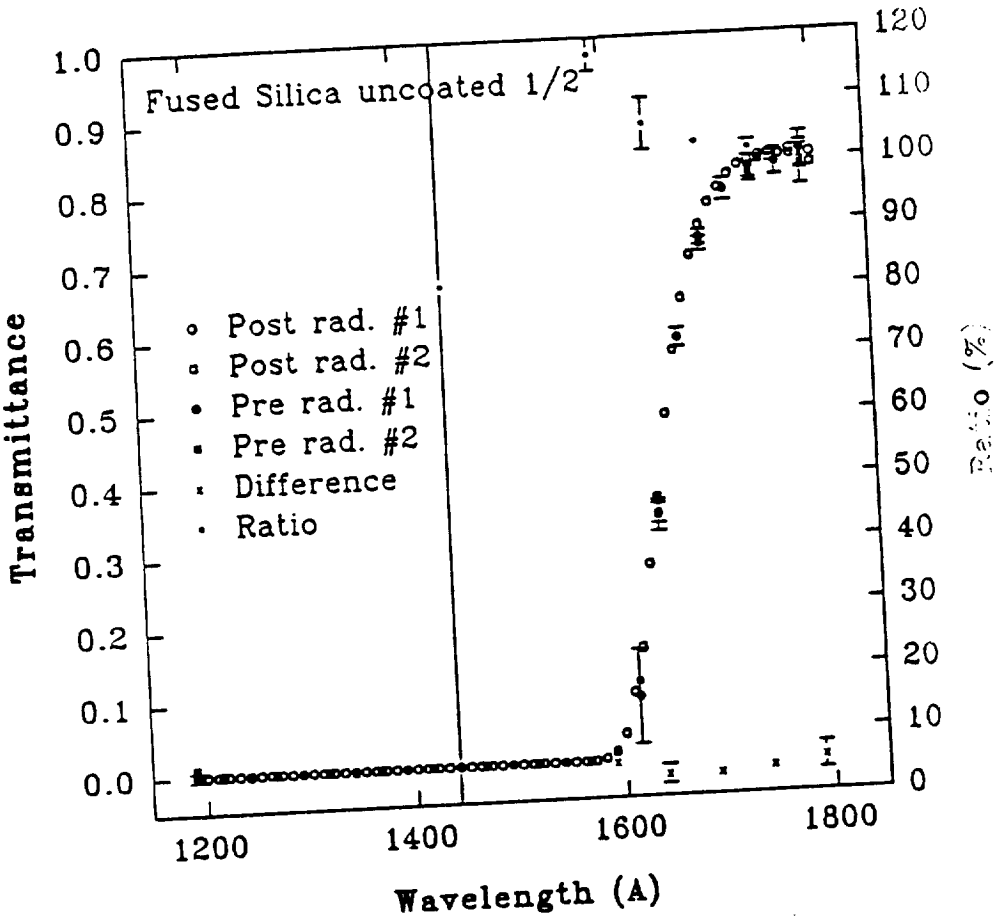
Fused Silica uncoated 1/2"
Post rad. #1
Post rad. #2
Pre rad. #1
Pre rad. #2
Difference
Ratio
Transmittance
Wavelength (A)
1.0
0.9
0.8
0.7
0.6
0.5
0.4
0.3
0.2
0.1
0.0
1200
1400
1600
1800
120
110
100
90
80
70
60
50
40
30
20
10
0

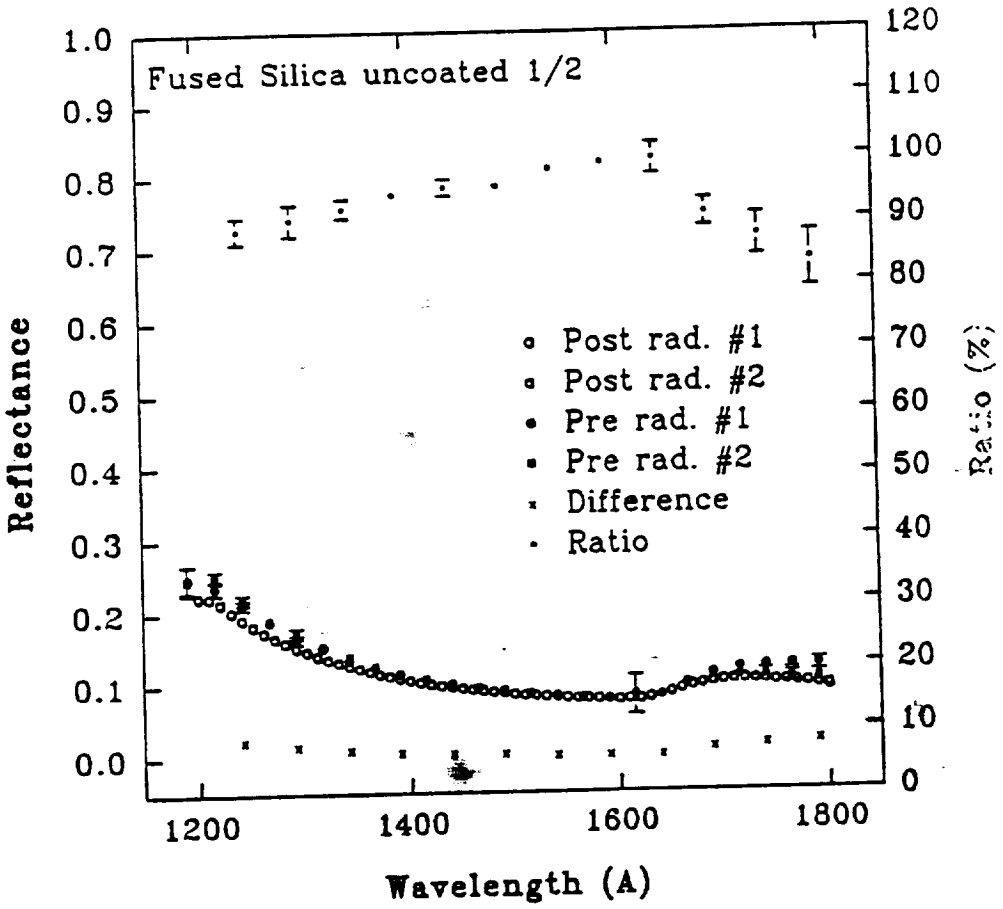

ORIGINAL PAGE IS
OF POOR QUALITY

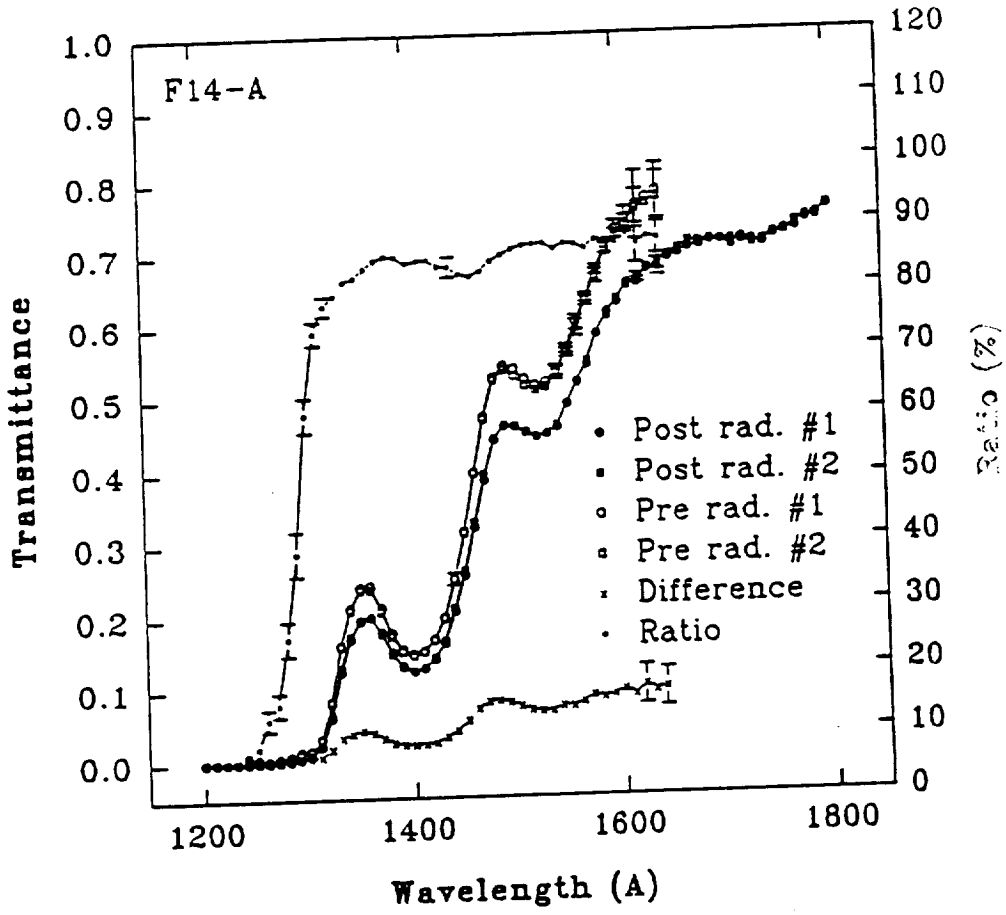
F14-A
Transmittance
Wavelength (A)
Ratio (%)
1.0
0.9
0.8
0.7
0.6
0.5
0.4
0.3
0.2
0.1
0.0
1200
1400
1600
1800
120
110
100
90
80
70
60
50
40
30
20
10
0
Post rad. #1
Post rad. #2
Pre rad. #1
Pre rad. #2
Difference
Ratio

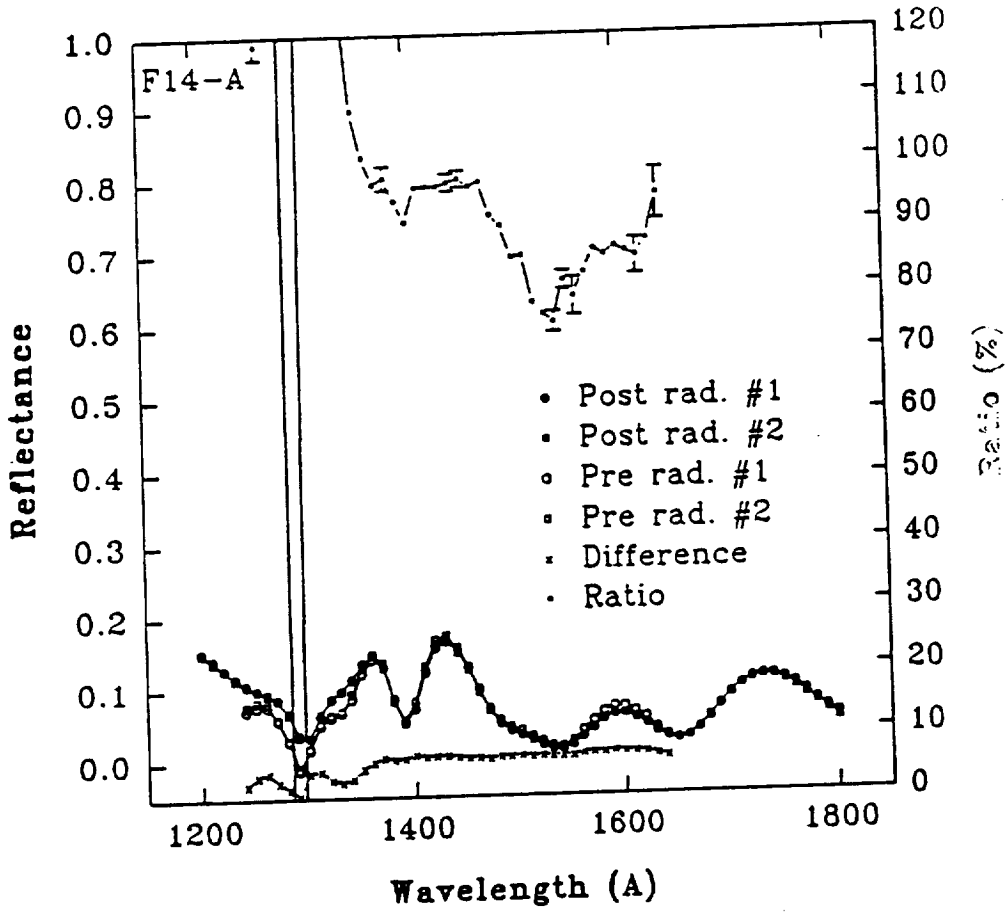
F14-A
Reflectance
Wavelength (A)
Ratio (%)
1.0
0.9
0.8
0.7
0.6
0.5
0.4
0.3
0.2
0.1
0.0
1200
1400
1600
1800
120
110
100
90
80
70
60
50
40
30
20
10
0
Post rad. #1
Post rad. #2
Pre rad. #1
Pre rad. #2
Difference
Ratio

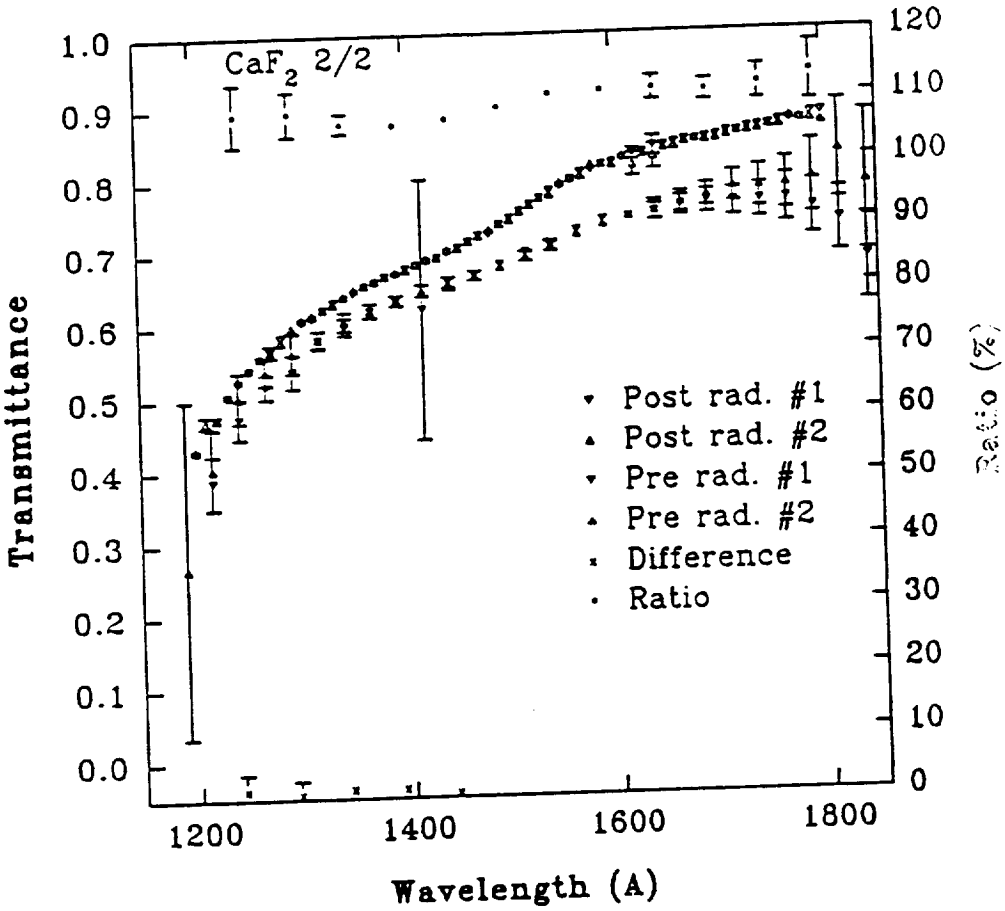
CaF2 2/2
Post rad. #1
Post rad. #2
Pre rad. #1
Pre rad. #2
Difference
Ratio
Transmittance
Wavelength (A)
Ratio (%)
1.0
0.9
0.8
0.7
0.6
0.5
0.4
0.3
0.2
0.1
0.0
120
110
100
90
80
70
60
50
40
30
20
10
0
1200
1400
1600
1800

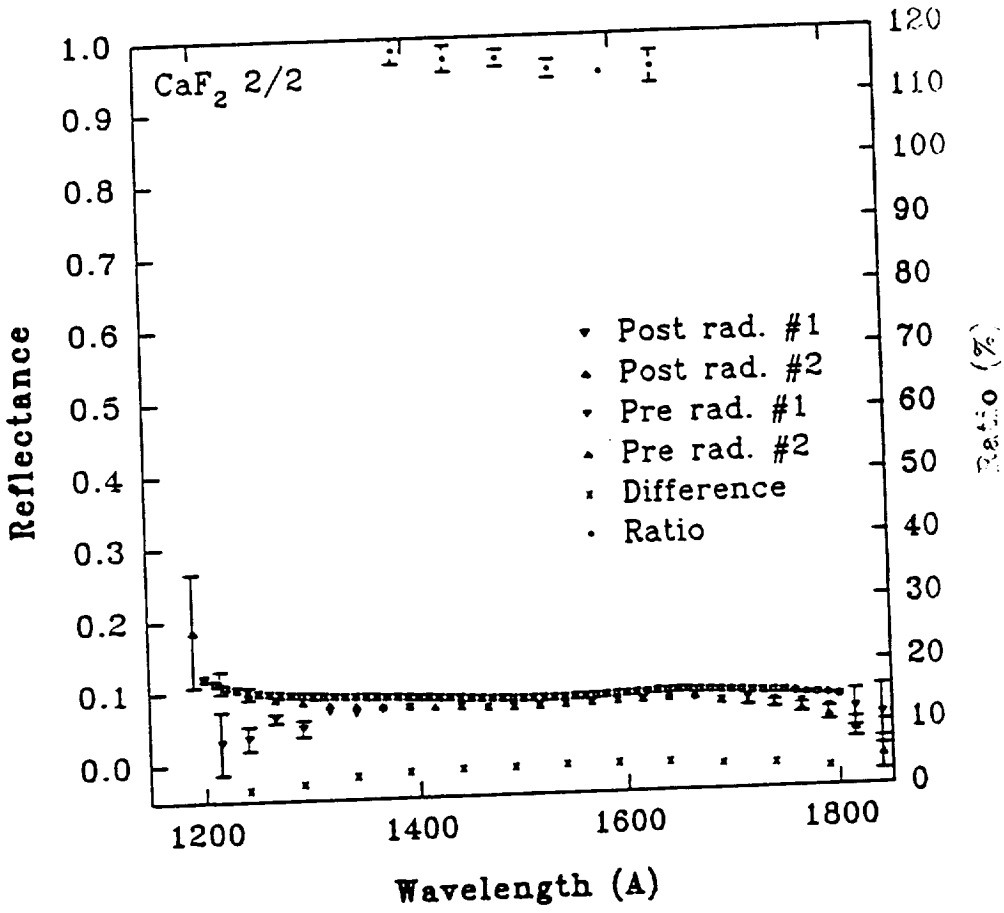
CaF2 2/2
Post rad. #1
Post rad. #2
Pre rad. #1
Pre rad. #2
Difference
Ratio
Reflectance
Wavelength (A)
1.0
0.9
0.8
0.7
0.6
0.5
0.4
0.3
0.2
0.1
0.0
120
110
100
90
80
70
60
50
40
30
20
10
0
1200
1400
1600
1800

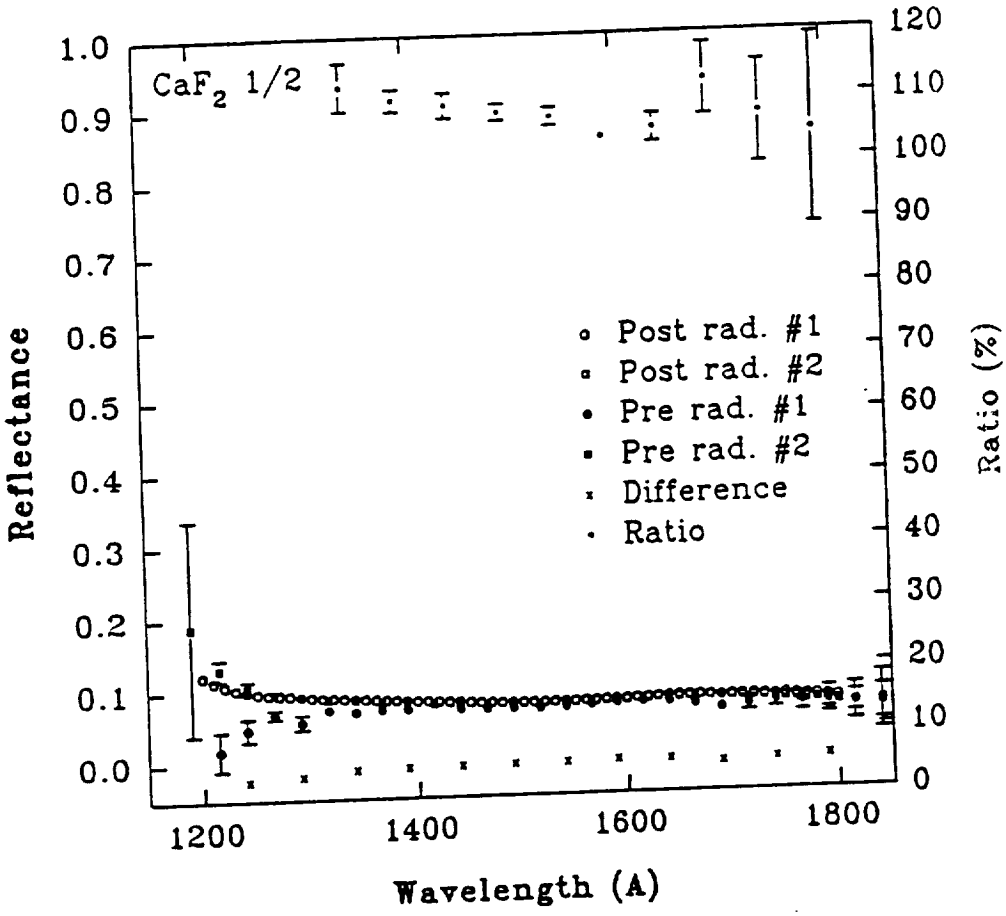

PRECEDING PAGE BLANK NOT FILMED

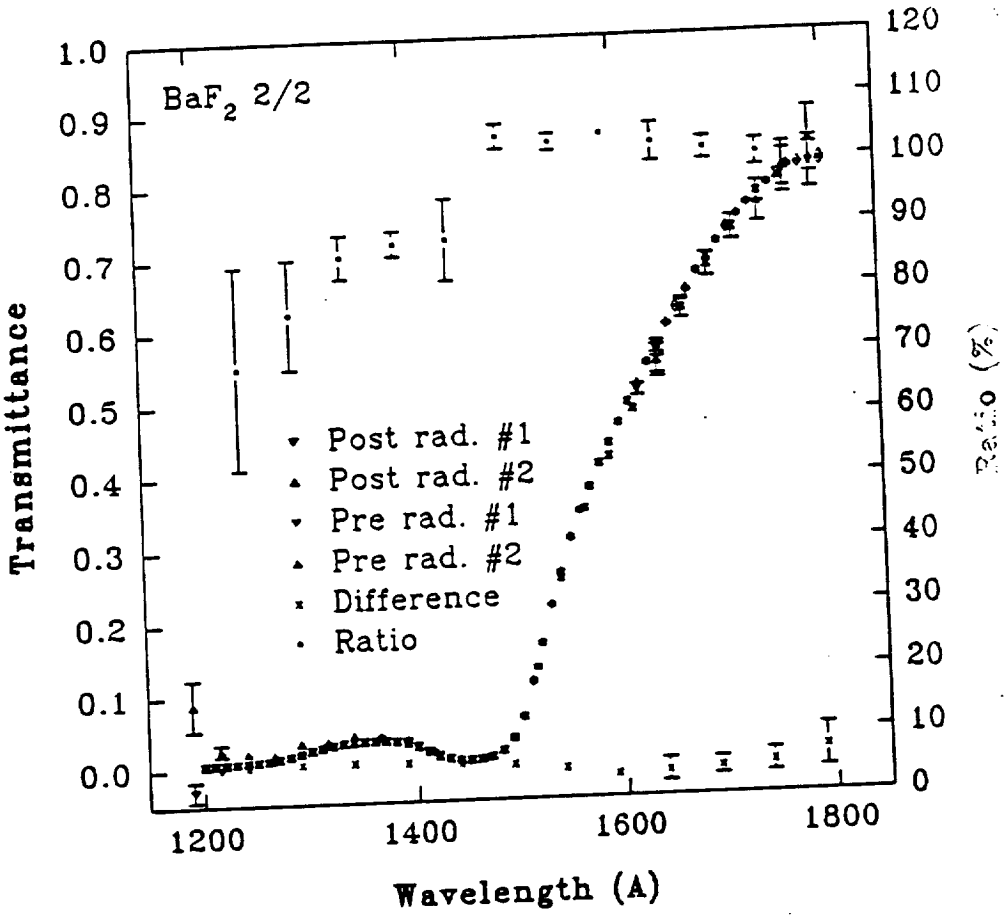
BaF2 2/2
Post rad. #1
Post rad. #2
Pre rad. #1
Pre rad. #2
Difference
Ratio
Transmittance
Wavelength (A)
Ratio (%)
1.0
0.9
0.8
0.7
0.6
0.5
0.4
0.3
0.2
0.1
0.0
120
110
100
90
80
70
60
50
40
30
20
10
0
1200
1400
1600
1800

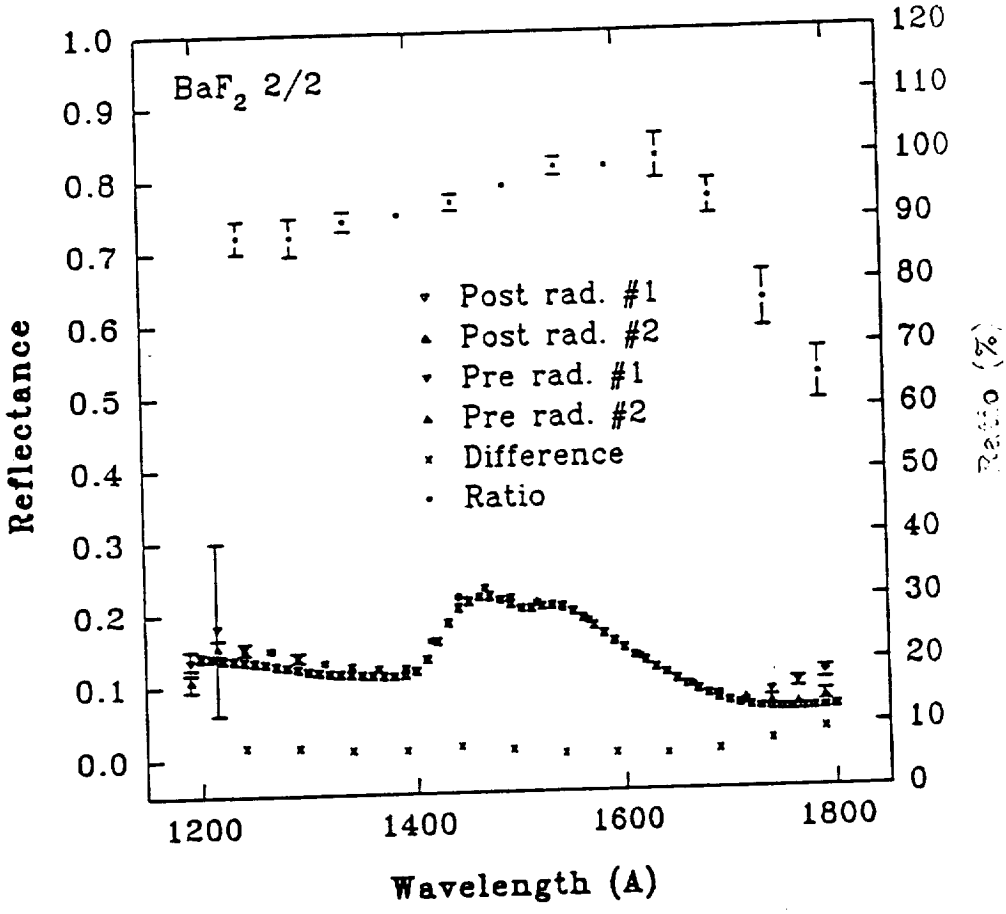
BaF2 2/2
Post rad. #1
Post rad. #2
Pre rad. #1
Pre rad. #2
Difference
Ratio
Reflectance
Wavelength (A)
Ratio (%)
1.0
0.9
0.8
0.7
0.6
0.5
0.4
0.3
0.2
0.1
0.0
120
110
100
90
80
70
60
50
40
30
20
10
0
1200
1400
1600
1800

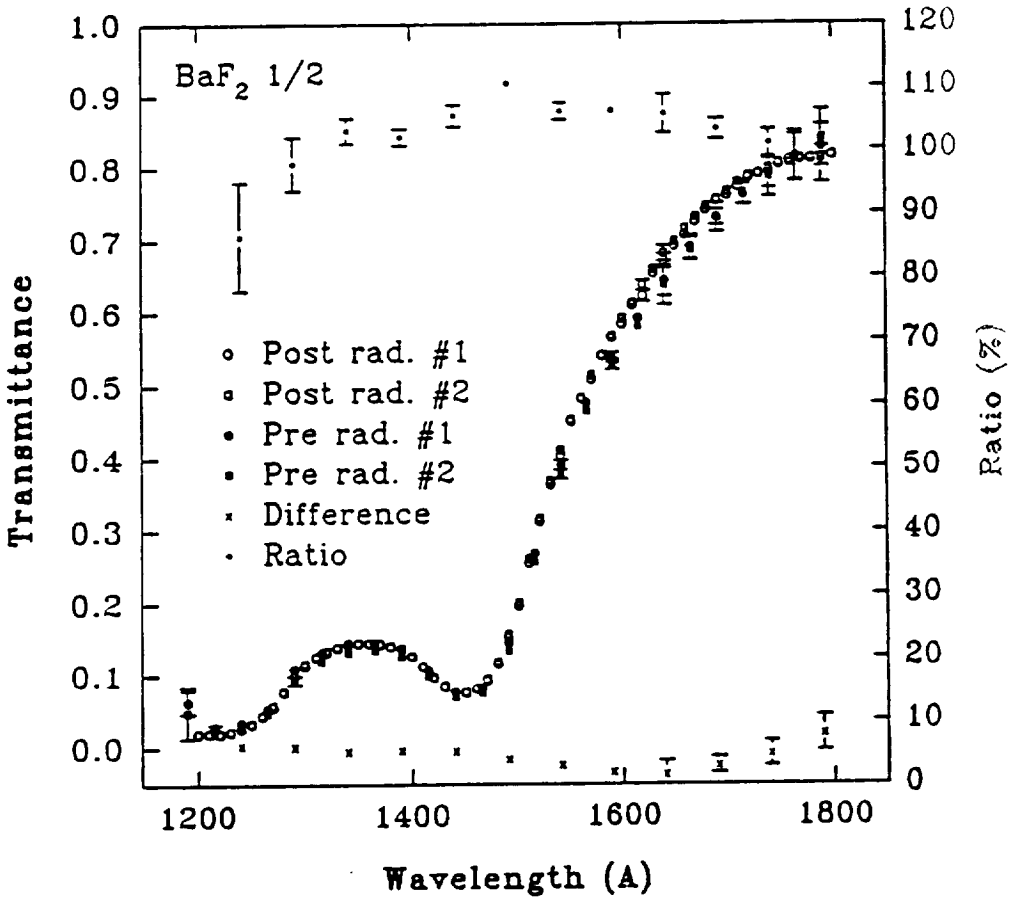
BaF2 1/2
Post rad. #1
Post rad. #2
Pre rad. #1
Pre rad. #2
Difference
Ratio
Transmittance
Ratio (%)
Wavelength (A)
1.0
0.9
0.8
0.7
0.6
0.5
0.4
0.3
0.2
0.1
0.0
120
110
100
90
80
70
60
50
40
30
20
10
0
1200
1400
1600
1800

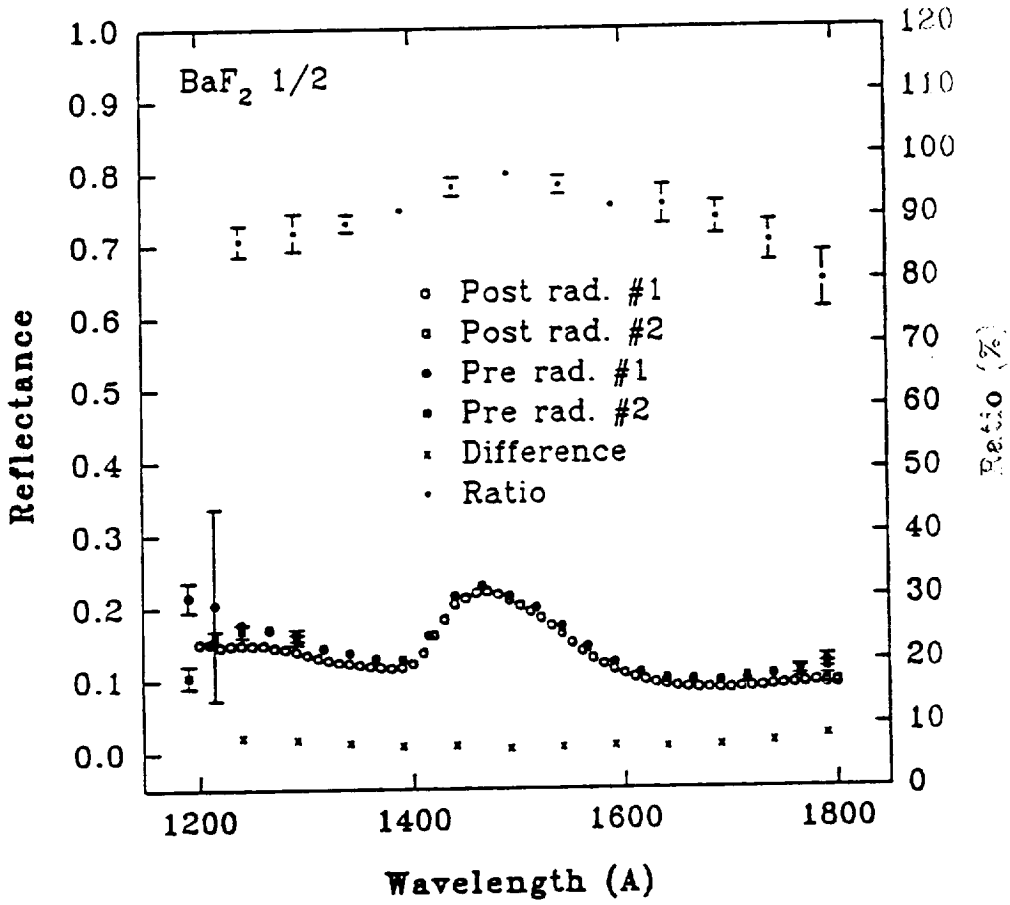
BaF2 1/2
Post rad. #1
Post rad. #2
Pre rad. #1
Pre rad. #2
Difference
Ratio
Reflectance
Ratio (%)
Wavelength (A)
1.0
0.9
0.8
0.7
0.6
0.5
0.4
0.3
0.2
0.1
0.0
120
110
100
90
80
70
60
50
40
30
20
10
0
1200
1400
1600
1800

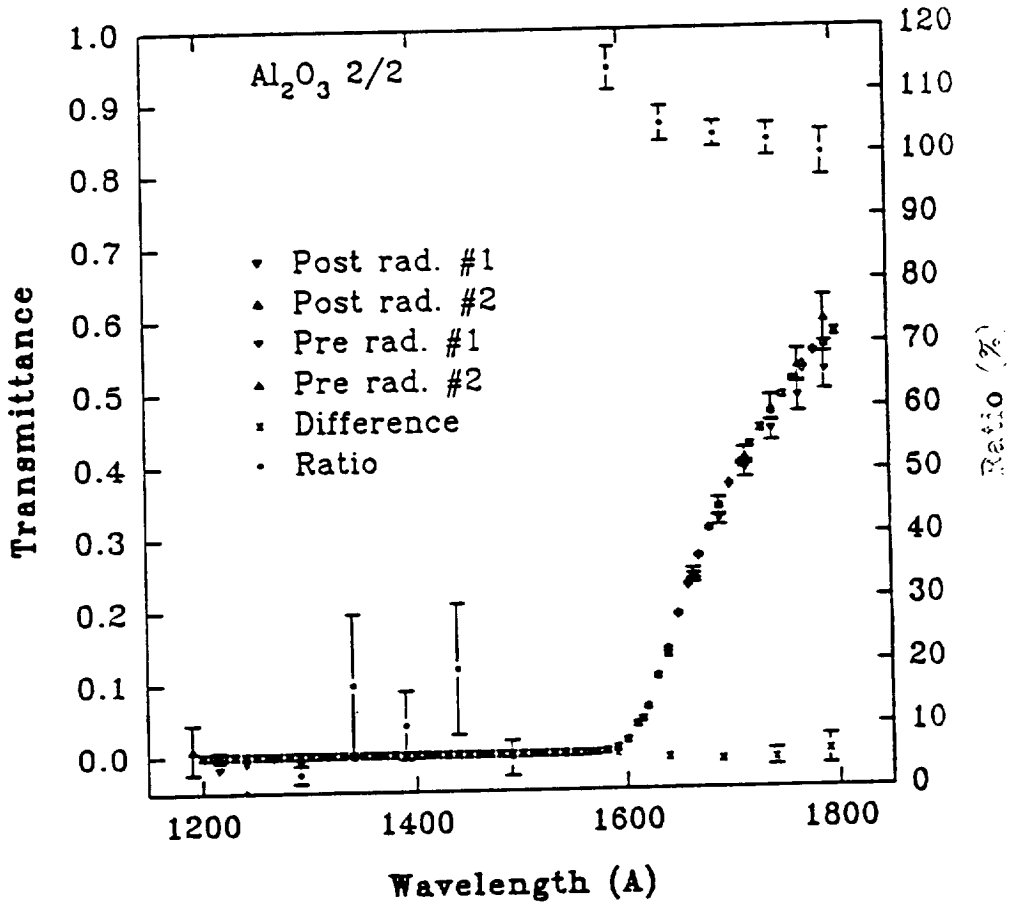
Al_2O_3 2/2
Post rad. #1
Post rad. #2
Pre rad. #1
Pre rad. #2
Difference
Ratio
Transmittance
Ratio (%)
Wavelength (A)
1.0
0.9
0.8
0.7
0.6
0.5
0.4
0.3
0.2
0.1
0.0
120
110
100
90
80
70
60
50
40
30
20
10
0
1200
1400
1600
1800

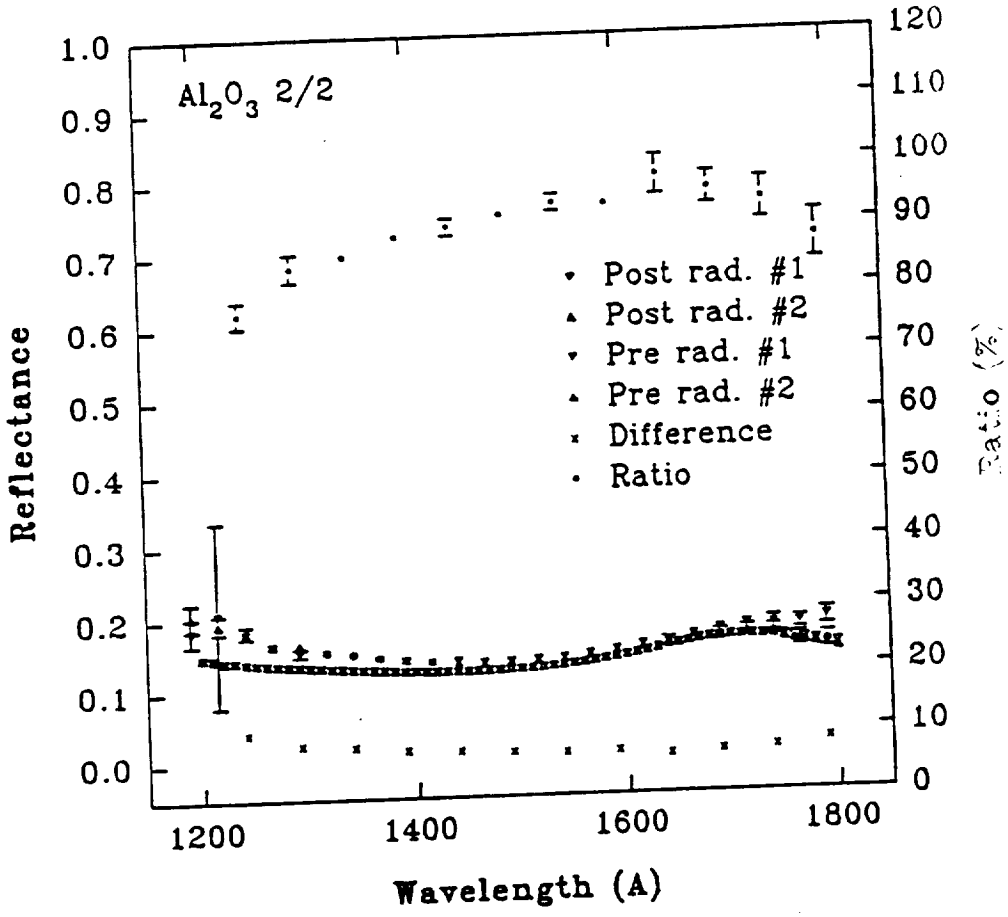
Al_2O_3 2/2
Post rad. #1
Post rad. #2
Pre rad. #1
Pre rad. #2
Difference
Ratio
Reflectance
Ratio (%)
Wavelength (A)
1.0
0.9
0.8
0.7
0.6
0.5
0.4
0.3
0.2
0.1
0.0
120
110
100
90
80
70
60
50
40
30
20
10
0
1200
1400
1600
1800

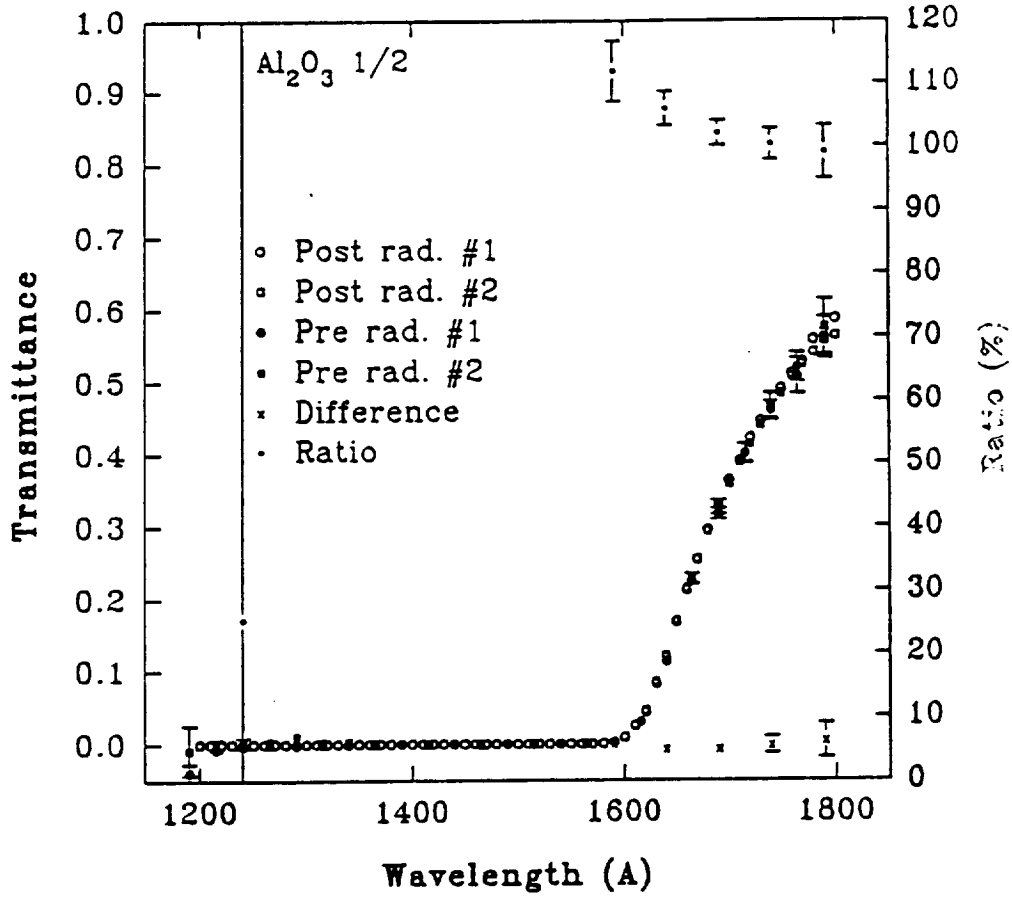
Al_2O_3 1/2
Post rad. #1
Post rad. #2
Pre rad. #1
Pre rad. #2
Difference
Ratio
Transmittance
Ratio (%)
Wavelength (A)
1.0
0.9
0.8
0.7
0.6
0.5
0.4
0.3
0.2
0.1
0.0
120
110
100
90
80
70
60
50
40
30
20
10
0
1200
1400
1600
1800

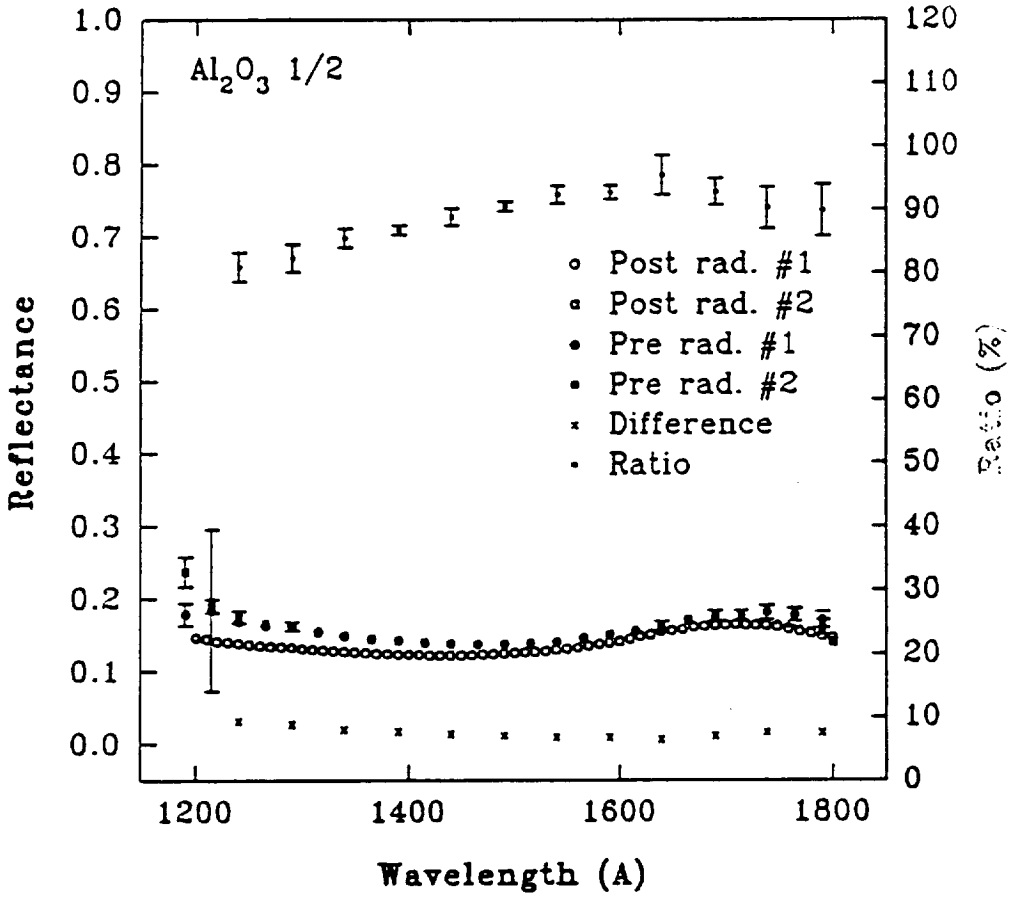
Al_2O_3 1/2
Post rad. #1
Post rad. #2
Pre rad. #1
Pre rad. #2
Difference
Ratio
Reflectance
Ratio (%)
Wavelength (A)
1.0
0.9
0.8
0.7
0.6
0.5
0.4
0.3
0.2
0.1
0.0
120
110
100
90
80
70
60
50
40
30
20
10
0
1200
1400
1600
1800

6. Appendix B - Semiannual Status Report

The University of Alabama in Huntsville

Semiannual Status Report for Grant NAG8-834
Due Date: December 24, 1991

"Theoretical and Experimental Studies Relevant to Interpretation of Auroral Emissions"

Submitted to

George C. Marshall Space Flight Center
Space Science Laboratory
National Aeronautics and Space Administration
Marshall Space Flight Center, AL 35812

by

Charles E. Keffer
Principal Investigator
The University of Alabama in Huntsville
Physics Department
Huntsville, AL 35899

Theoretical and Experimental Studies Relevant to Interpretation of Auroral Emissions

1 Introduction

Work under this contract is divided into two tasks. Task one is a laboratory study designed to improve our understanding of the space vehicle induced external environment and its effect on measurement of auroral emissions from space-based platforms. Task two is a modeling program to develop the capability of using auroral images at various wavelengths to infer the total energy influx and characteristic energy of the incident auroral particles. Together they provide a significant contribution to the field of space-based auroral imaging.

2 Space Vehicle Contamination Study

The laboratory study has begun to focus on studying the impact of the space environment on the Ultraviolet Imager (UVI). The radiation environment for the Polar orbiting UVI is very harsh. We have initiated a study, which will be completed within the next six months, of radiation effects on the thin films used in developing the flight filters for the UVI. Also, we are currently completing a series of tests on the effect of the thermal space environment on the UVI. Summaries of both of these studies will be included in this report.

2.1 Thin Film Measurements

The filters being developed for the Ultraviolet Imager will be exposed to a severe radiation environment in space during the duration of the UVI mission. It is unknown to what extent, if any, this radiation environment will damage the filters in flight. So, we are performing a test to measure the effects from the anticipated dose of radiation. Briefly, we have selected 14 single layer thin films, 4 uncoated substrates, and 4 multilayer filters for radiation testing. The thin films, substrates, and multilayer filters are typical of the materials and filters which will be used in the flight version of the UVI. Seven of the single layer thin films, 2 uncoated substrates, and all of the multilayer filters will be exposed to the anticipated dose of radiation with the remainder of the samples serving as control cases.

A series of reflectance and transmittance measurements has been performed on each of the samples mentioned above. For the reflectance measurements, two identical scans from 1200 Å to 1800 Å were performed on each sample prior to its radiation exposure. A single filter (RF135L/GII) was measured as a control on every set of reflectance measurements to check the reliability and reproducibility of the data from scan to scan. The RF135L/GII control insured that no systematic errors were introduced when the vacuum chamber was vented and a new set of samples was installed. Two identical scans from 1200 Å to 1800 Å were also performed on each sample, prior to radiation exposure, during the transmittance measurements. The MgF_2 17 filter was measured on every transmittance measurement as a check on the scan to scan reliability and

PRECEDING PAGE BLANK NOT FILMED

reproducibility. Figures 1 and 2 show typical reflectance and transmittance measurements, respectively.

All of the samples, with the exception of the 9 controls, have been sent to Goddard Space Flight Center where they will be exposed to a radiation dose equivalent to what they are expected to experience during the duration of the ISTP Polar mission. Following completion of this radiation exposure, the samples will be returned and the reflectance and transmittance measurements will be repeated. A determination will be made at that time as to whether any degradation in filter performance is anticipated from exposure of the UVI flight filters to the radiation environment of space.

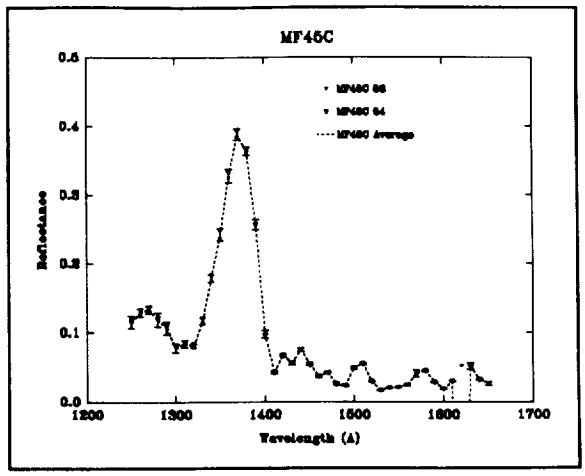

Figure 1. This figure shows two reflectance measurements of the filter MF45C.

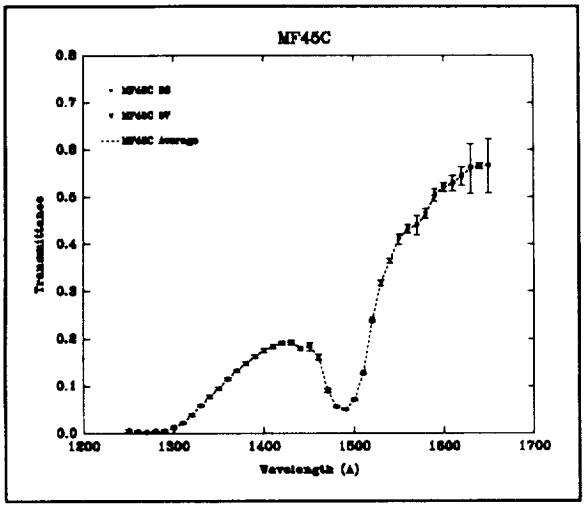

Figure 2. This figure shows two transmittance measurements of the filter MF45C.

2.2 UVI Thermal Test

The Ultraviolet Imager is passively cooled by radiative heat transfer from the instrument to the 3 °K thermal background of space. The performance of the UVI in this thermal environment of space is a key factor in the success of the mission. We have, therefore, designed and carried out a phase one test of the UVI camera thermal performance.

A test setup was built which was designed to simulate the thermal environment of the UVI on orbit. For this purpose, the UVI engineering model was assembled to be as much like the final flight version as was presently possible. Also, the VUV calibration vacuum chamber was configured to simulate the thermal/vacuum environment of space. The UVI camera was mounted on a baseplate cooled/heated over the nominal temperature range of -20 °C to 30 °C by a recirculating water/ethanol mixture. A second cold plate was suspended approximately 2" above the UVI camera's passive radiator. This cold plate was painted black and the radiator was black anodized to increase their emissivities and thus improve the radiative heat transfer from the UVI to the cold plate. Liquid nitrogen could be flowed through the cold plate so that its temperature approached 77 °K.

Several key questions were addressed in this phase one thermal test. Will the CCD reach its operational target temperature of ≤ -55 °C? Can the optical bench be maintained near room

temperature with 10 watts of available heater power? Will the electronics remain sufficiently warm during survival mode conditions? Do the "hot" electronic parts have adequate cooling? With the exception of CCD operational temperature, all key questions were answered in the affirmative. Discussions at the Ultraviolet Imager Thermal Design Review on December 19, 1991 concluded that some differences between the engineering model and the flight version of the UVI camera could account for the deviation of approximately 5 °C from the CCD target temperature. Follow up thermal tests during the next six months will seek to resolve the outstanding thermal environment interaction issues.

3 Auroral Modeling

Modeling activities through the end of CY 1991 included developing an ionospheric conductivity algorithm, updating FLIP and auroral code models, beginning high latitude FLIP modifications, and supporting the second UVI science workshop for discussion of analysis of auroral images.

3.1 Global Modeling

One of the original goals of the modeling program was to integrate the auroral code with the FLIP global ionospheric model. With the recent implementation of new versions of both models, this goal is complete. The FLIP model now accepts auroral production data as one of its standard inputs, allowing concurrent modeling of dayglow and auroral emissions. The newest versions of the codes use ASCII intermediate files, allowing operation of the codes on several different platforms. Presently, the codes are available for use on the MSFC CRAY and SSL VAX computer systems.

In addition, we've modified the auroral code to include an important additional source of auroral 1356 Å emission. This additional source, dissociative excitation of O_2, leads to a factor of two change for an incident 10 keV auroral flux. The latest version of the auroral code also allows simple photoelectron sources to be included with the auroral emission sources. For selected emissions, this allows concurrent modeling of dayglow and auroral emissions without invoking the much larger FLIP code.

3.2 High Latitude Modifications

To be used successfully at auroral latitudes, the FLIP model must be modified to take account of several high latitude mechanisms. We are currently developing an F-region plasma convection model to allow the FLIP model to include plasma drift due to ionospheric electric fields. Plasma convection throughout the polar region can significantly alter the plasma densities relative to a static model which has the feet of the flux tubes anchored to the Earth's surface. We are adapting the convection model of Sojka, Rasmussen, and Schunk (J. Geophys. Res., 91, 11281, 1986). Among its other features, the convection model includes a dependence on the direction of the interplanetary magnetic field. Development of the convection algorithm is approximately 50% complete.

3.3 Conductivity Calculations

Ionospheric conductivities are central to an understanding of the coupled ionosphere-thermosphere-magnetosphere. We've added the calculation of ionospheric conductivities to the combined FLIP and auroral codes. Based on this algorithm development, we can now determine column integrated conductivities from measured FUV auroral emissions. We remove much of the variability of the modeled conductances by selecting an especially stable emission ratio such as LBH 1464/LBH 1838. Our previous modeling has demonstrated that the LBH emission ratio changes very little in response to seasonal and solar cyclic model perturbations. This stability is reflected in the modeled conductivities.

Current conductivity models tend to lack small scale temporal and spatial structure, due primarily to the relative lack of experimental data from which to calculate ionospheric conductivities. By calculating the conductivities relative to a remotely measurable observable (the LBH ratio), we allow future FUV optical measurements to supplement the existing models. Details of the conductivity calculation along with studies of the sensitivity of the conductivities to changes in characteristic energy, solar activity, and neutral composition have been submitted to the Journal of Geophysical Research for publication. In addition, the conductivity calculations were discussed in an oral presentation at the Fall Meeting of the American Geophysical Union (December 12, 1991; San Francisco).

3.4 UVI Workshops

The second Ultraviolet Imager (UVI) workshop was held on August 1,2 1991. The workshop allowed each of the attendees to participate in the mission science planning and to address their specific science requirements for the UVI instrument. A major focus of the workshop was a review of available thermospheric/ionospheric modeling and image analysis techniques.

The attendees included nationally prominent scientists in the fields of ionospheric and magnetospheric physics and chemistry. The workshop participants and agenda are given in Table 1.

Dr. Germany was responsible for coordination of the meeting, which was held in Salt Lake City, Utah. His responsibilities included arrangement of meeting facilities, communication with the science team members, and preparation of post workshop mailings. In addition, Dr. Germany participated in the workshop discussions and gave a presentation on the extraction of auroral parameters from auroral images via auroral modeling.

Agenda	
August 1, 1991	August 2, 1991
Program Status and Introduction	Automated Auroral Image Analysis
Goals for Auroral Imaging	VUV Calibration Source
Extraction of Parameters from Images	Update on Data Analysis
Improved Neutral Wind Modeling	Summary
Auroral Measurements and Models	
Attendees	
Dr. Joe Ajello	Jet Propulsion Laboratory
Dr. Ken Clark	University of Washington
Dr. Keith Cole	La Trobe University, Australia
Dr. Glynn Germany	University of Alabama in Huntsville
Dr. Phil Richards	University of Alabama in Huntsville
Dr. Ramin Samadani	Stanford University
Dr. Stan Solomon	University of Colorado
Dr. Doug Torr	University of Alabama in Huntsville
Dr. Marsha Torr	NASA/MSFC

Table 1. Attendees and agenda of the UVI workshop.